

Exact Potts Model Partition Functions on Strips of the Honeycomb Lattice

Shu-Chiuan Chang* and Robert Shrock**

C. N. Yang Institute for Theoretical Physics
State University of New York
Stony Brook, N. Y. 11794-3840

Abstract

We present exact calculations of the partition function of the q -state Potts model on (i) open, (ii) cyclic, and (iii) Möbius strips of the honeycomb (brick) lattice of width $L_y = 2$ and arbitrarily great length. In the infinite-length limit the thermodynamic properties are discussed. The continuous locus of singularities of the free energy is determined in the q plane for fixed temperature and in the complex temperature plane for fixed q values. We also give exact calculations of the zero-temperature partition function (chromatic polynomial) and $W(q)$, the exponent of the ground-state entropy, for the Potts antiferromagnet for honeycomb strips of type (iv) $L_y = 3$, cyclic, (v) $L_y = 3$, Möbius, (vi) $L_y = 4$, cylindrical, and (vii) $L_y = 4$, open. In the infinite-length limit we calculate $W(q)$ and determine the continuous locus of points where it is nonanalytic. We show that our exact calculation of the entropy for the $L_y = 4$ strip with cylindrical boundary conditions provides an extremely accurate approximation, to a few parts in 10^5 for moderate q values, to the entropy for the full 2D honeycomb lattice (where the latter is determined by Monte Carlo measurements since no exact analytic form is known).

*email: shu-chiuan.chang@sunysb.edu

**email: robert.shrock@sunysb.edu

1 Introduction

The q -state Potts model has served as a valuable model for the study of phase transitions and critical phenomena [1, 2]. On a lattice, or, more generally, on a (connected) graph G , at temperature T , this model is defined by the partition function

$$Z(G, q, v) = \sum_{\{\sigma_n\}} e^{-\beta\mathcal{H}} \quad (1.1)$$

with the (zero-field) Hamiltonian

$$\mathcal{H} = -J \sum_{\langle ij \rangle} \delta_{\sigma_i \sigma_j} \quad (1.2)$$

where $\sigma_i = 1, \dots, q$ are the spin variables on each vertex (site) $i \in G$; $\beta = (k_B T)^{-1}$; and $\langle ij \rangle$ denotes pairs of adjacent vertices. The graph $G = G(V, E)$ is defined by its vertex set V and its edge set E ; we denote the number of vertices of G as $n = n(G) = |V|$ and the number of edges of G as $e(G) = |E|$. We use the notation

$$K = \beta J, \quad a = u^{-1} = e^K, \quad v = a - 1 \quad (1.3)$$

so that the physical ranges are (i) $a \geq 1$, i.e., $v \geq 0$ corresponding to $\infty \geq T \geq 0$ for the Potts ferromagnet, and (ii) $0 \leq a \leq 1$, i.e., $-1 \leq v \leq 0$, corresponding to $0 \leq T \leq \infty$ for the Potts antiferromagnet. One defines the (reduced) free energy per site $f = -\beta F$, where F is the actual free energy, via

$$f(\{G\}, q, v) = \lim_{n \rightarrow \infty} \ln[Z(G, q, v)^{1/n}]. \quad (1.4)$$

where we use the symbol $\{G\}$ to denote $\lim_{n \rightarrow \infty} G$ for a given family of graphs. In the present context, this $n \rightarrow \infty$ limit corresponds to the limit of infinite length for a strip graph of the honeycomb lattice of fixed width and some prescribed boundary conditions.

Let $G' = (V, E')$ be a spanning subgraph of G , i.e. a subgraph having the same vertex set V and an edge set $E' \subseteq E$. Then $Z(G, q, v)$ can be written as the sum [3]-[5]

$$\begin{aligned} Z(G, q, v) &= \sum_{G' \subseteq G} q^{k(G')} v^{e(G')} \\ &= \sum_{r=k(G)}^{n(G)} \sum_{s=0}^{e(G)} z_{rs} q^r v^s \end{aligned} \quad (1.5)$$

where $k(G')$ denotes the number of connected components of G' and $z_{rs} \geq 0$. Since we only consider connected graphs G , we have $k(G) = 1$. The formula (1.5) enables one to generalize q from \mathbb{Z}_+ to \mathbb{R}_+ (keeping v in its physical range). This generalization is sometimes denoted the random cluster model [5, 6]; here we shall use the term ‘‘Potts model’’ to include both positive integral q as in the original formulation in eqs. (1.1) and (1.2), and the generalization to real (or complex) q , via eq. (1.5). The formula (1.5) shows that $Z(G, q, v)$ is a polynomial in q and v (equivalently, a) with maximum and minimum degrees indicated in eq. (1.5). The Potts model partition function on a graph G is essentially equivalent to the Tutte polynomial [7]-[9] and Whitney rank polynomial [4], [2], [10]-[12] for this graph, as discussed in the appendix.

In this paper we shall present exact calculations of the Potts model partition function for strips of the honeycomb (equivalently, brick) lattice of width $L_y = 2$ vertices and arbitrary length equal to m bricks, with

boundary conditions of the following types: (i) $(FBC_y, FBC_x) =$ free or open, (ii) $(FBC_y, PBC_x) =$ cyclic, and (iii) $(FBC_y, TPBC_x) =$ Möbius, where FBC and $(T)PBC$ refer to free and (twisted) periodic boundary conditions, respectively, and the longitudinal and transverse directions are taken to be \hat{x} (horizontal) and \hat{y} (vertical). This is a natural extension to the honeycomb lattice of our previous exact calculations of Potts model partition functions on finite-width, arbitrary-length strips of other lattices [13]-[17]. Note that while the Potts model partition functions, or equivalently, Tutte polynomials for the limit of infinite 2D triangular and honeycomb lattices are simply related by duality, this is not true for finite-width strips of the triangular and honeycomb lattices, owing to boundary effects. (Dual graphs are discussed further in the appendix.) In addition to these results for arbitrary temperature, we present exact calculations for the interesting case of the zero-temperature antiferromagnet for strips of the honeycomb lattice of the following types: (iv) $L_y = 3$, cyclic, (v) $L_y = 3$, Möbius, (vi) $L_y = 4$, $(PBC_y, FBC_x) =$ cylindrical, and (vii) $L_y = 4$, free.

There are several motivations for these exact calculations of Potts model partition functions for strips of the honeycomb lattice. Clearly, new exact calculations of Potts model partition functions are of value in their own right. From these, in the limit of infinite-length strips, one derives exact thermodynamic functions and can make rigorous comparisons of various properties among strips of different lattices, e.g., square, honeycomb, and triangular. In particular, with these exact results one can study both the $T = 0$ critical point of the q -state Potts ferromagnet and $T = 0$ properties of the Potts antiferromagnet. Further, we shall use our exact results to study how, for a given value of q , the ground state degeneracy per site (exponent of the ground state entropy per site) for the Potts antiferromagnet approaches its value for the infinite honeycomb lattice. We shall show that the exactly determined function for the ground state degeneracy calculated for the strip with an infinite-length strip with a rather modest width of $L_y = 4$ and cylindrical boundary conditions is already an extremely good approximation, for a wide range of q values, to the corresponding function for the full 2D honeycomb lattice (the latter being determined by Monte Carlo measurements). This is very useful since no exact expression for the ground state degeneracy per site for $q > 2$ is known for the 2D honeycomb lattice. In addition, it was shown [14] that these calculations can give insight into the complex-temperature phase diagram of the 2D Potts model on the given lattice, which is again useful since, except for the $q = 2$ Ising case, the latter phase diagrams are not known exactly. Finally, via the correspondence with the Tutte polynomial, our calculations yield several quantities of relevance to mathematical graph theory.

Various special cases of the Potts model partition function are of interest. One special case is the zero-temperature limit of the Potts antiferromagnet. For sufficiently large q , on a given lattice or graph G , this exhibits nonzero ground state entropy (without frustration). This is of interest as an exception to the third law of thermodynamics [18, 19]. This is equivalent to a ground state degeneracy per site (vertex), $W > 1$, since $S_0 = k_B \ln W$. The $T = 0$ (i.e., $v = -1$) partition function of the above-mentioned q -state Potts antiferromagnet on G satisfies

$$Z(G, q, -1) = P(G, q) \tag{1.6}$$

where $P(G, q)$ is the chromatic polynomial (in q) expressing the number of ways of coloring the vertices of the graph G with q colors such that no two adjacent vertices have the same color [3, 10, 20, 21]. The minimum number of colors necessary for this coloring is the chromatic number of G , denoted $\chi(G)$. We have

$$W(\{G\}, q) = \lim_{n \rightarrow \infty} P(G, q)^{1/n} . \tag{1.7}$$

At certain special points q_s (typically $q_s = 0, 1, \dots, \chi(G)$), one has the noncommutativity of limits

$$\lim_{q \rightarrow q_s} \lim_{n \rightarrow \infty} P(G, q)^{1/n} \neq \lim_{n \rightarrow \infty} \lim_{q \rightarrow q_s} P(G, q)^{1/n} \tag{1.8}$$

and hence it is necessary to specify the order of the limits in the definition of $W(\{G\}, q_s)$ [22].

Using the formula (1.5) for $Z(G, q, v)$, one can generalize q from \mathbb{Z}_+ not just to \mathbb{R}_+ but to \mathbb{C} and a from its physical ferromagnetic and antiferromagnetic ranges $1 \leq a \leq \infty$ and $0 \leq a \leq 1$ to $a \in \mathbb{C}$. A subset of the zeros of Z in the two-complex dimensional space \mathbb{C}^2 defined by the pair of variables (q, a) can form an accumulation set in the $n \rightarrow \infty$ limit, denoted \mathcal{B} , which is the continuous locus of points where the free energy is nonanalytic. This locus is determined as the solution to a certain $\{G\}$ -dependent equation [13, 14]. For a given value of a , one can consider this locus in the q plane, and we denote it as $\mathcal{B}_q(\{G\}, a)$. In the special case $a = 0$ (i.e., $v = -1$) where the partition function is equal to the chromatic polynomial, the zeros in q are the chromatic zeros, and $\mathcal{B}_q(\{G\}, a = 0)$ is their continuous accumulation set in the $n \rightarrow \infty$ limit. In previous papers we have given exact calculations of the chromatic polynomials and nonanalytic loci \mathcal{B}_q for various families of graphs; some of these are related earlier works are [22]-[26]-[48] (see [14] for further references). With the exact Potts partition function for arbitrary temperature, one can study \mathcal{B}_q for $a \neq 0$ and, for a given value of q , one can study the continuous accumulation set of the zeros of $Z(G, q, v)$ in the a plane; this will be denoted $\mathcal{B}_a(\{G\}, q)$. It will often be convenient to consider the equivalent locus in the $u = 1/a$ plane, namely $\mathcal{B}_u(\{G\}, q)$. We shall sometimes write $\mathcal{B}_q(\{G\}, a)$ simply as \mathcal{B}_q or \mathcal{B} when $\{G\}$ and a are clear from the context, and similarly with \mathcal{B}_a and \mathcal{B}_u . One gains a unified understanding of the separate loci $\mathcal{B}_q(\{G\})$ for fixed a and $\mathcal{B}_a(\{G\})$ for fixed q by relating these as different slices of the locus \mathcal{B} in the \mathbb{C}^2 space defined by (q, a) as we shall do here.

Following the notation in [22] and our other earlier works on $\mathcal{B}_q(\{G\})$ for $a = 0$, we denote the maximal region in the complex q plane to which one can analytically continue the function $W(\{G\}, q)$ from physical values where there is nonzero ground state entropy as R_1 . The maximal value of q where \mathcal{B}_q intersects the (positive) real axis was labelled $q_c(\{G\})$. Thus, region R_1 includes the positive real axis for $q > q_c(\{G\})$. Correspondingly, in our works on complex-temperature properties of spin models, we had labelled the complex-temperature extension (CTE) of the physical paramagnetic phase as (CTE)PM, which will simply be denoted PM here, the extension being understood, and similarly with ferromagnetic (FM) and antiferromagnetic (AFM); other complex-temperature phases, having no overlap with any physical phase, were denoted O_j (for ‘‘other’’), with j indexing the particular phase [49, 50]. Here we shall continue to use this notation for the respective slices of \mathcal{B} in the q and a or u planes. Various special cases of $Z(G, q, v)$ applicable for arbitrary graphs G were given in [14].

Just as one must take account of the noncommutativity in the definition of W , eq. (1.8), so also one must take account of noncommutativity in the definition of the free energy: at certain special points q_s (typically $q_s = 0, 1, \dots, \chi(G)$) one has

$$\lim_{n \rightarrow \infty} \lim_{q \rightarrow q_s} Z(G, q, v)^{1/n} \neq \lim_{q \rightarrow q_s} \lim_{n \rightarrow \infty} Z(G, q, v)^{1/n} . \quad (1.9)$$

Because of this noncommutativity, the formal definition (1.4) is, in general, insufficient to define the free energy f at these special points q_s ; it is necessary to specify the order of the limits that one uses in eq. (1.9). We denote the two definitions using different orders of limits as f_{qn} and f_{nq} :

$$f_{nq}(\{G\}, q, v) = \lim_{n \rightarrow \infty} \lim_{q \rightarrow q_s} n^{-1} \ln Z(G, q, v) \quad (1.10)$$

$$f_{qn}(\{G\}, q, v) = \lim_{q \rightarrow q_s} \lim_{n \rightarrow \infty} n^{-1} \ln Z(G, q, v) . \quad (1.11)$$

In Ref. [22] and our subsequent works on chromatic polynomials and the above-mentioned zero-temperature antiferromagnetic limit, it was convenient to use the ordering $W(\{G\}, q_s) = \lim_{q \rightarrow q_s} \lim_{n \rightarrow \infty} P(G, q)^{1/n}$

since this avoids certain discontinuities in W that would be present with the opposite order of limits. In the present work on the full temperature-dependent Potts model partition function, we shall consider both orders of limits and comment on the differences where appropriate. Of course in discussions of the usual q -state Potts model (with positive integer q), one automatically uses the definition in eq. (1.1) with (1.2) and no issue of orders of limits arises, as it does in the Potts model with real q . Consequences of the noncommutativity (1.9) have been discussed before [14, 16, 17].

As derived in [14], a general form for the Potts model partition function for the strip graphs G_s considered here, or more generally, for recursively defined families of graphs comprised of m repeated subunits (e.g. the columns of squares of height L_y vertices that are repeated $L_x = m$ times to form an $L_x \times L_y$ strip of a regular lattice with some specified boundary conditions), is

$$Z((G_s)_m, q, v) = \sum_{j=1}^{N_{Z, G_s, \lambda}} c_{Z, G_s, j} (\lambda_{Z, G_s, j}(q, v))^m \quad (1.12)$$

where $N_{Z, G_s, \lambda}$, $c_{Z, G_s, j}$, and $\lambda_{Z, G_s, j}$ depend on the type of recursive family G_s (lattice structure and boundary conditions) but not on its length m . For special case of the $T = 0$ antiferromagnet, the partition function, or equivalently, the chromatic polynomial $P((G_s)_m, q)$ has the corresponding form

$$P((G_s)_m, q) = \sum_{j=1}^{N_{P, G_s, \lambda}} c_{P, G_s, j} (\lambda_{P, G_s, j}(q, v))^m . \quad (1.13)$$

For sufficiently large integer q values, the coefficients can be interpreted as multiplicities of eigenvalues of coloring matrices [42], and the sums of these coefficients are thus sums of dimensions of invariant subspaces of these matrices. For a given family G_s of strip graphs we shall denote these sums as

$$C_{Z, G_s} = \sum_{j=1}^{N_{Z, G_s, \lambda}} c_{Z, G_s, j} \quad (1.14)$$

and

$$C_{P, G_s} = \sum_{j=1}^{N_{P, G_s, \lambda}} c_{P, G_s, j} . \quad (1.15)$$

Here we distinguish the quantities $N_{Z, G_s, \lambda}$, $N_{P, G_s, \lambda}$; $c_{Z, G_s, j}$, $c_{P, G_s, j}$; $\lambda_{Z, G_s, j}$, and $\lambda_{P, G_s, j}$. Below, for brevity of notation, we shall sometimes suppress the Z or P subscripts and the s subscript on G_s when the meaning is clear from context and no confusion will result.

The Potts ferromagnet has a zero-temperature phase transition in the $L_x \rightarrow \infty$ limit of the strip graphs considered here, and this has the consequence that for cyclic and Möbius boundary conditions, \mathcal{B} passes through the $T = 0$ point $u = 0$. It follows that \mathcal{B} is noncompact in the a plane. Hence, it is usually more convenient to study the slice of \mathcal{B} in the $u = 1/a$ plane rather than the a plane. For the ferromagnet, since $a \rightarrow \infty$ as $T \rightarrow 0$ and Z diverges like $a^{e(G_s)}$ in this limit, we shall use the reduced partition function Z_r defined by

$$Z_r((G_s)_m, q, v) = a^{-e((G_s)_m)} Z((G_s)_m, q, v) = u^{e((G_s)_m)} Z((G_s)_m, q, v) \quad (1.16)$$

which has the finite limit $Z_r \rightarrow q$ as $T \rightarrow 0$. For a general strip graph $(G_s)_m$ of type G_s and length $L_x = m$, we can write

$$Z_r((G_s)_m, q, v) = u^{e((G_s)_m)} \sum_{j=1}^{N_{Z, G_s, \lambda}} c_{Z, G_s, j} (\lambda_{Z, G_s, j})^m \equiv \sum_{j=1}^{N_{Z, G_s, \lambda}} c_{Z, G_s, j} (\lambda_{Z, G_s, j, u})^m \quad (1.17)$$

with

$$\lambda_{Z, G_s, j, u} = u^{e((G_s)_m)/m} \lambda_{Z, G_s, j} . \quad (1.18)$$

For the Potts model partition functions of the $L_y = 2$ cyclic and Möbius strips of the honeycomb lattice to be discussed below, the prefactor in eq. (1.18) is u^5 .

For the following, it will be convenient to define some general functions. First, we define the following polynomial:

$$D_k(q) = \frac{P(C_k, q)}{q(q-1)} = \sum_{s=0}^{k-2} (-1)^s \binom{k-1}{s} q^{k-2-s} \quad (1.19)$$

and $P(C_n, q)$ is the chromatic polynomial for the circuit (cyclic) graph C_n with n vertices, given by $P(C_n, q) = (q-1)^n + (q-1)(-1)^n$.

Second, we define coefficients of degree d in q which are related to Chebyshev polynomials:

$$c^{(d)} = U_{2d} \left(\frac{\sqrt{q}}{2} \right) \quad (1.20)$$

where $U_n(x)$ is the Chebyshev polynomial of the second kind, defined by

$$U_n(x) = \sum_{j=0}^{\lfloor \frac{n}{2} \rfloor} (-1)^j \binom{n-j}{j} (2x)^{n-2j} \quad (1.21)$$

where in eq. (1.21) the notation $\lfloor \frac{n}{2} \rfloor$ in the upper limit on the summand means the integral part of $\frac{n}{2}$. The first few of these coefficients are

$$c^{(0)} = 1 , \quad c^{(1)} = q - 1 , \quad (1.22)$$

$$c^{(2)} = q^2 - 3q + 1, \quad (1.23)$$

and

$$c^{(3)} = q^3 - 5q^2 + 6q - 1 . \quad (1.24)$$

2 Chromatic Polynomial for the $L_y = 2$ Cyclic and Möbius Strips of the Honeycomb Lattice

Before giving our calculation of the Potts model partition functions for these strips, it is useful to discuss a particularly interesting special case, namely that of the zero-temperature antiferromagnet. For the open strip of m bricks, which will be denoted S_m for short,

$$P(hc, 2 \times m, FBC_y, FBC_x, q) = q(q-1)(D_6)^m = q(q-1)(q^4 - 5q^3 + 10q^2 - 10q + 5)^m \quad (2.1)$$

so that in the $m \rightarrow \infty$ limit,

$$W(hc, 2 \times \infty, FBC_y, FBC_x, q) = (q^4 - 5q^3 + 10q^2 - 10q + 5)^{1/4} . \quad (2.2)$$

Since this has only discrete branch point singularities at the zeros of D_6 , the continuous locus $\mathcal{B} = \emptyset$.

The chromatic polynomials for width $L_y = 2$ cyclic and Möbius strips of the honeycomb lattice can be obtained as special cases of the calculations in [38] for homeomorphic expansions of cyclic and Möbius strips of the square lattice. These homeomorphic expansions involved the addition of $k-2$ degree-2 vertices

on the upper and lower horizontal edges of the strips, thereby making cyclic or Möbius strips of p -gons with $p = 2k$ such that two successive p -gons intersected on one common edge. Here, the degree Δ (i.e., coordination number) of a vertex in a graph G is defined as the number of edges (bonds) that connect to it. The case $k = 3$, i.e., $p = 6$, was thus the width 2 cyclic or Möbius strip of the honeycomb lattice, depending on the longitudinal boundary conditions. We denote these strips as $L_m = hc, 2 \times m, FBC_y, PBC_x$ and $ML_m = hc, 2 \times m, FBC_y, TPBC_x$ for short. For quantities that are independent of the value of m in L_m or ML_m , we shall use the notation L and ML . The graphs L_m and ML_m have $n = 4m$ vertices. For m large enough to avoid degenerate cases (i.e. $m \geq 2$ for the cyclic strip and $m \geq 1$ for the Möbius strip), the chromatic number for the $L_y \times m$ strips of the honeycomb lattice with cyclic boundary conditions is

$$\chi(hc, L_y \times m, FBC_y, PBC_x) = 2 \quad (2.3)$$

while for the Möbius strips we have

$$\chi(hc, L_y \times m, FBC_y, TPBC_x) = 3 \quad (2.4)$$

independent of m in the indicated ranges.

The results for the chromatic polynomials (in our current notation) are [38]

$$P(hc, 2 \times m, FBC_y, PBC_x, q) = \sum_{j=1}^4 c_{P,L,j} (\lambda_{P,L,j})^m \quad (2.5)$$

and

$$P(hc, 2 \times m, FBC_y, TPBC_x, q) = \sum_{j=1}^4 c_{P,ML,j} (\lambda_{P,L,j})^m \quad (2.6)$$

where, as indicated, the $\lambda_{P,G,j}$'s are the same for cyclic and Möbius strips [38, 43]:

$$\lambda_{P,L,1} = 1 \quad (2.7)$$

$$\lambda_{P,L,2} = D_4 + D_3 = (q-1)^2 \quad (2.8)$$

$$\lambda_{P,L,3} = D_4 - D_3 = q^2 - 4q + 5 \quad (2.9)$$

$$\lambda_{P,L,4} = D_6 = q^4 - 5q^3 + 10q^2 - 10q + 5 . \quad (2.10)$$

The corresponding coefficients are

$$c_{P,L,1} = c^{(2)} \quad (2.11)$$

$$c_{P,L,2} = c_{P,L,3} = c^{(1)} \quad (2.12)$$

$$c_{P,L,4} = c^{(0)} = 1 \quad (2.13)$$

$$c_{P,ML,1} = -c^{(0)} = -1 \quad (2.14)$$

$$c_{P,ML,2} = -c^{(1)} \quad (2.15)$$

$$c_{P,ML,3} = c^{(1)} \quad (2.16)$$

$$c_{P,ML,4} = c^{(0)} = 1 . \quad (2.17)$$

The equality of the coefficients (here, $c_{P,L,4}$ and $c_{P,ML,4}$) of the $\lambda_{G,j}$ that is dominant in region R_1 , independent of longitudinal boundary conditions, is a general result [43, 13].

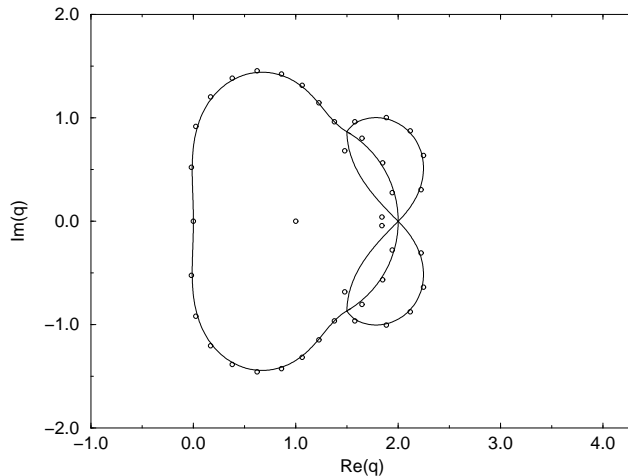


Figure 1: Locus \mathcal{B}_q for the $m \rightarrow \infty$ limit of the cyclic $L_y = 2$ strip $\{L\}$ of the honeycomb lattice with $a = 0$. Zeros of $Z(L_m, q, v = -1) = P(L_m, q)$ for $m = 20$, i.e., $n = 80$ vertices, are shown for comparison.

The singular locus \mathcal{B} was given as Fig. 1(a) in [38]. For our current generalization to nonzero temperature, it will be necessary to refer to details of this locus, so we show it as Fig. 1. As is evident in this figure, the locus (boundary) \mathcal{B} separates the q plane into six regions: (i) R_1 containing the real intervals $q > q_c = 2$ and $q < 0$ and extending outward to complex infinity, (ii) an innermost region R_2 containing the real interval $0 < q < q_c$, and two complex conjugate pairs of regions, (iii) R_3, R_3^* to the upper and lower right of q_c , and (iv) R_4, R_4^* to the upper and lower left of q_c . The dominant terms in these regions are (i) $\lambda_{P,L,4}$ in R_1 , (ii) $\lambda_{P,L,3}$ in R_2 , (iii) $\lambda_{P,L,2}$ in R_3, R_3^* , and (iv) $\lambda_{P,L,1}$ in R_4, R_4^* . The point q_c is a multiple point where six curves, forming three branches of \mathcal{B} , cross. This corresponds to the fact that at q_c there is a degeneracy in magnitude of all of the $\lambda_{P,L,j}$'s. The angles at which the various boundary curves emanates from q_c are: (a) $\pi/4$ for the curve separating R_1 and R_3 , (b) $\pi/2$ for the curve separating R_3 from R_4 , and (c) $3\pi/4$ for the curve separating R_4 from R_2 , and so forth for the complex-conjugate curves. The density of chromatic zeros is small on the boundary separating R_2 and R_4 , and its complex conjugate boundary. The locus \mathcal{B} has support for $Re(q) < 0$ as well as $Re(q) \geq 0$. Further, some chromatic zeros for finite- m strips and a portion of the locus \mathcal{B} for the $m \rightarrow \infty$ limit both lie within the circle $|q - 1| = 1$. This is also true for the $L_y = 3$ cyclic and Möbius strips of the honeycomb lattice (see below). In this context, we recall that the conjecture later made in [46, 45] that chromatic zeros and, in the limit of infinite-length, the locus \mathcal{B} , do not lie in the interior of the circle $|q - 1|$ was stated to be specific to strips of the square and triangular lattice.

The W function in these regions is given by

$$W = (D_6)^{1/4} \quad \text{for } q \in R_1 \quad (2.18)$$

$$|W| = |q^2 - 4q + 5|^{1/4} \quad \text{for } q \in R_2 \quad (2.19)$$

$$|W| = |q - 1|^{1/2} \quad \text{for } q \in R_3, R_3^* \quad (2.20)$$

$$|W| = 1 \quad \text{for } q \in R_4, R_4^* . \quad (2.21)$$

Recall that for regions other than R_1 , only the magnitude of W can be determined unambiguously [22]. Note that $W(q = 2) = 1$. We next generalize this study to the case of finite temperature for both the antiferromagnet and the ferromagnet.

3 Potts Model Partition Function for Open $L_y = 2$ Strip of the Honeycomb Lattice

By using an iterative application of the deletion-contraction theorem for Tutte polynomials and converting the result to Z , or by using a transfer matrix method, one can calculate the partition function for the open, cyclic, and Möbius strips of the honeycomb lattice of width L_y and arbitrary length m bricks, which we shall again denote as S_m , L_m , and ML_m . We have used both methods. These calculations are a natural extension of our earlier calculations of Potts model partition functions for finite-width lattice strips of arbitrarily great length [13], [14]-[17]. We begin with the open strip. The results are conveniently expressed in terms of a generating function

$$\Gamma_Z(S_m, q, v) = \sum_{m=0}^{\infty} Z(S_m, q, v) z^m . \quad (3.1)$$

We find

$$\Gamma_Z(S_m, q, v) = \frac{A_{S,0} + A_{S,1}z}{(1 - \lambda_{Z,S,1}z)(1 - \lambda_{Z,S,2}z)} \quad (3.2)$$

where

$$A_{S,0} = q(q + v) \quad (3.3)$$

$$A_{S,1} = -q^2 v^4 (1 + v) \quad (3.4)$$

$$\lambda_{Z,S,(1,2)} = \frac{1}{2}(T_S \pm \sqrt{R_S}) \quad (3.5)$$

with

$$T_S = v^5 + 6v^4 + 10qv^3 + 10q^2v^2 + 5q^3v + q^4 \quad (3.6)$$

$$\begin{aligned} R_S = & 4qv^8 - 4q^2v^7 - 6q^3v^6 - 2q^4v^5 + v^{10} + 32v^8 + 8v^9 + 104v^7q \\ & + 196v^6q^2 + 244v^5q^3 + 208v^4q^4 + q^8 + 10q^7v + 45q^6v^2 + 120q^5v^3 . \end{aligned} \quad (3.7)$$

The equivalent Tutte polynomial $T(S_m, x, y)$ is given in the appendix.

We have studied the locus \mathcal{B} in the \mathbb{C}^2 space defined by the variables (q, v) (or equivalently, (q, a)). For $a = 0$, Z reduces to the chromatic polynomial (2.1), and the resultant W function, given in eq. (2.2) has only discrete branch point singularities at the zeros of D_6 (namely, $q \simeq 0.690983 \pm 0.9510565i$ and $1.809017 \pm 0.587785i$), and consequently $\mathcal{B} = \emptyset$. As a initially increases from 0, \mathcal{B}_q consists of arcs that spread out from these four points. An illustrative case, $a = 0.1$, is shown in Fig. 2. As $a \rightarrow 1$, these arcs shrink in toward the origin, $q = 0$.

In Figs. 3 and 4 we show \mathcal{B}_u for $q = 2$ and 3, respectively. The positive real u axis, and the region reached by analytic continuation from it, form the (CTE)PM phase. Since the infinite-length, finite-width

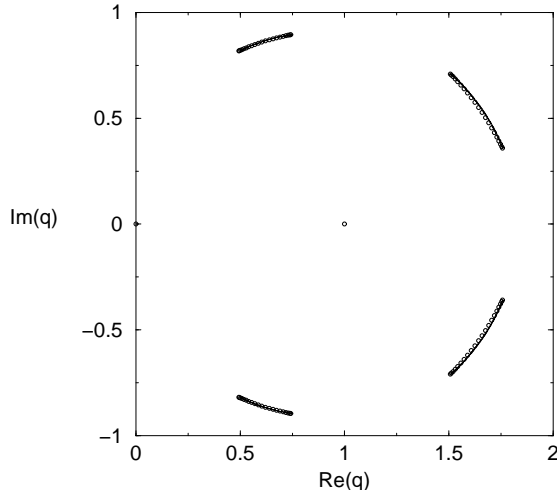


Figure 2: Locus \mathcal{B}_q for the $n \rightarrow \infty$ limit of the $L_y = 2$ honeycomb strip $\{S\}$ with free longitudinal boundary conditions, for $a = v + 1 = 0.1$. Zeros of $Z(S_m, q, v = -0.9)$ for $m = 21$, i.e., $n = 86$ vertices, are shown for comparison.

strips are quasi-one-dimensional systems and the spin-spin couplings are short-range (specifically, nearest-neighbor), an elementary application of a Peierls argument shows that there is no long-range order and thus no broken-symmetry (FM or AFM) phases at any finite temperature. Related to this, the singular locus \mathcal{B}_u does not cross the positive real u axis.

4 Thermodynamic Properties of the Potts Model on the $2 \times \infty$ Strip of the Honeycomb Lattice

We next discuss the physical thermodynamic properties of the q -state Potts model on the $2 \times \infty$ strip of the honeycomb lattice. These are independent of the longitudinal boundary conditions. The reduced free energy per site is given (with the f_{nq} definition) by

$$f = \frac{1}{4} \ln \lambda_{Z,S,1} . \quad (4.1)$$

This is analytic for all finite temperature for both signs of the spin-spin coupling (ferromagnetic and anti-ferromagnetic). This analyticity property is equivalent to the above-mentioned fact that the singular locus \mathcal{B}_u does not cross the positive real u axis. It is straightforward to calculate from this the internal energy U and specific heat C per site. These have the high-temperature expansions

$$U = -\frac{5J}{4q} \left[1 + \left(\frac{q-1}{q} \right) K + O(K^2) \right] \quad (4.2)$$

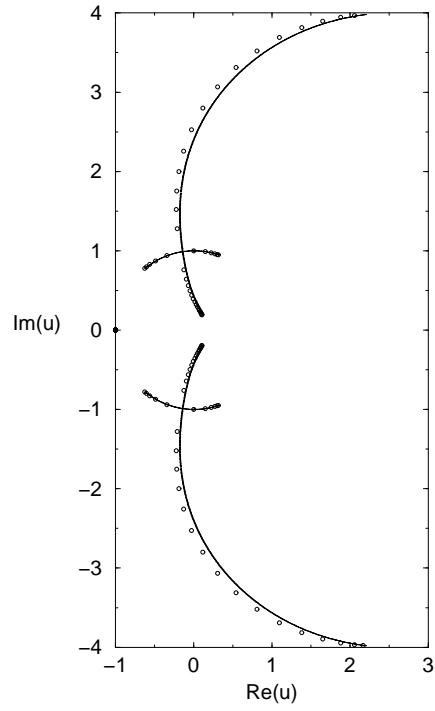


Figure 3: Locus \mathcal{B}_u for the $m \rightarrow \infty$ limit of the $L_y = 2$ strip of the honeycomb lattice with free longitudinal boundary conditions, $\{S\}$ with $q = 2$. Zeros of $Z(S_m, q = 2, v)$ in u for $m = 21$ (so that Z is a polynomial of degree 106 in v and hence, up to an overall factor, in u) are shown for comparison.

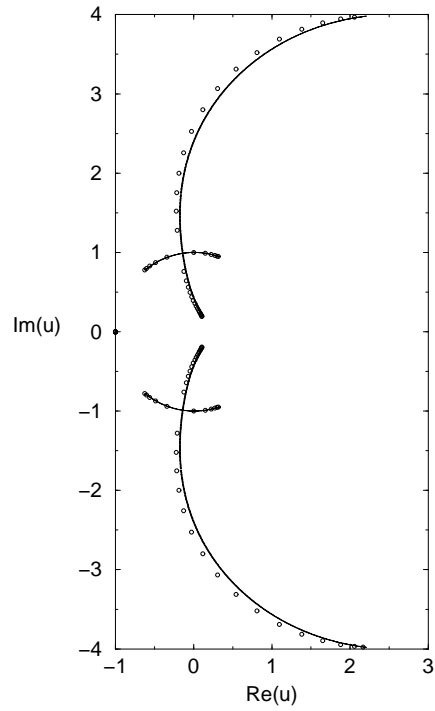


Figure 4: Locus \mathcal{B}_u : same as in Fig. 3 for $q = 3$.

$$C = \frac{5k_B(q-1)K^2}{4q^2} \left[1 + \left(\frac{q-2}{q} \right) K + O(K^2) \right]. \quad (4.3)$$

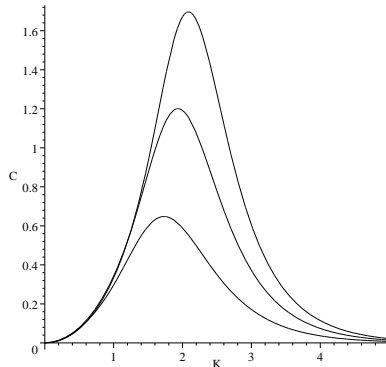


Figure 5: Specific heat C/k_B for the q -state Potts ferromagnet on the $2 \times \infty$ strip of the honeycomb lattice as a function of $K = J/(k_B T)$. From bottom to top the curves are for $q = 2, 3, 4$.

In Fig. 5 we show a plot of the specific heat for the ferromagnetic case. One sees that as q increases, the value of K at which the maximum in the specific heat occurs increases; i.e. this maximum occurs at lower temperature. This is a consequence of the fact that the spins are “floppier” for larger q , and hence one must cool the system to lower temperatures in order to achieve short-range ordering (as noted above, there is, of course, no long-range ordering). Further, as q increases, the height of the maximum increases. This can be interpreted as a result of the fact that as one makes q larger, one increases the effective number of degrees of freedom per site, and it is the onset of short-range ordering of these degrees of freedom that produces the maximum in the specific heat.

It is also of interest to compare our exact calculations of the specific heat for the $2 \times \infty$ strip of the honeycomb lattice with our previous calculations for the $2 \times \infty$ strips of the square and triangular lattices. In Fig. 6 we show this comparison for the Ising case $q = 2$. One sees that the value of K at which the maximum occurs increases as one goes from triangular to square to honeycomb lattices. This is a consequence of the fact that the short-range ordering in the spins is strengthened as one increases the effective coordination number (vertex degree) of the lattice strip. The cyclic $L_y = 2$ strips of the square and triangular lattices are Δ -regular, i.e., each vertex has the same degree, namely $\Delta = 3$ and $\Delta = 4$, respectively. This is also true of the infinite-length limit of the open $L_y = 2$ strips of the square and triangular lattices. For the $L_y = 2$ strip of the honeycomb lattice, and more generally, for a graph G and its $n \rightarrow \infty$ limit $\{G\}$, it is useful to define the effective coordination number (degree) as

$$\Delta_{eff}(\{G\}) = \lim_{n(G) \rightarrow \infty} \frac{2e(G)}{n(G)}. \quad (4.4)$$

For the infinite-length limit of the $L_y = 2$ strip of the honeycomb lattice, half of the vertices have degree 2 and half have degree 3, so that the effective coordination number is 2.5. Thus, since one increases the (effective) coordination number from 2.5 to 3 to 4 going from the honeycomb to square to triangular $L_y = 2$ strips, one can achieve short-range order at a progressively higher temperature (smaller value of K). The same qualitative comparison applies for $q = 3, 4$, etc.

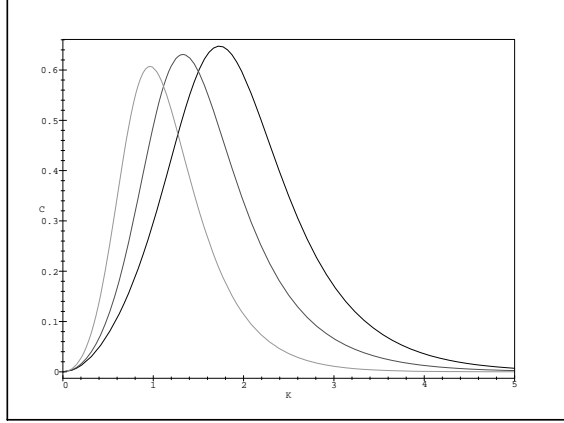


Figure 6: Comparison of the specific heat C/k_B (vertical axis) for the q -state Potts ferromagnet on the $2 \times \infty$ lattice strips for the Ising case, $q = 2$. In order of increasing position K_{max} of the maxima in these curves, they apply for the (a) triangular, (b) square, and (c) honeycomb.

Since the Potts ferromagnet has a $T = 0$ critical point on infinite-length, finite-width strips, it is worthwhile to examine the critical singularities. The specific heat has the low-temperature behavior

$$C = 6k_B K^2 (q-1) e^{-2K} \left[1 + \frac{3}{2} (q+2) e^{-K} + O(e^{-2K}) \right] \quad \text{as } K \rightarrow \infty . \quad (4.5)$$

Thus, as is typical of systems at their lower critical dimensionality and was true of the other finite-width, infinite-length strips for which we have performed exact calculations [14, 16, 17], the specific heat exhibits an essential zero at $T = 0$ as a function of temperature. In general, at a critical point the ratio ρ of the largest subdominant to the dominant λ_j 's determines the asymptotic decay of the connected spin-spin correlation function and hence the correlation length

$$\xi = -\frac{1}{\ln \rho} . \quad (4.6)$$

Since $\lambda_{Z,L,5}$ and $\lambda_{Z,L,3}$ are the dominant and leading subdominant $\lambda_{Z,G,j}$'s, respectively, we have

$$\rho_{FM} = \frac{\lambda_{Z,L,3}}{\lambda_{Z,L,5}} \quad (4.7)$$

and hence for the ferromagnetic zero-temperature critical point we find that the correlation length diverges, as $T \rightarrow 0$, as

$$\xi_{FM} \sim q^{-1} e^{2K} + O(e^K) , \quad \text{as } K \rightarrow \infty . \quad (4.8)$$

Again, this is an essential singularity (divergence) as a function of temperature, as is generic for systems at their lower critical dimensionality. The detailed form of the exponent is similar to the behavior $\xi \sim q^{-1} e^{2K}$ of the correlation length at the $T = 0$ critical point of the Potts ferromagnet on the $L_y = 2$ infinite-length strip of the square lattice [14]. While the correlation lengths for other 1D or quasi-1D systems also exhibit divergences with essential singularities, the detailed form of the exponent (coefficient of K) varies. Thus, for

example, $\xi_{FM} \sim q^{-1}e^K$ as $K \rightarrow \infty$ for the 1D Potts ferromagnet, while $\xi_{FM} \sim q^{-1}e^{3K}$ and $\xi_{FM} \sim q^{-1}e^{4K}$ as $K \rightarrow \infty$ for the Potts ferromagnet on the $L_y = 2$ strips of the triangular lattice [16] and on the square lattice with next-nearest-neighbor spin-spin couplings, respectively.

Except for the $q = 2$ Ising case, where, as is true on any bipartite lattice, there is an elementary equivalence between the ferromagnetic and antiferromagnetic signs of the spin-spin coupling J , the q -state Potts antiferromagnet on the $2 \times \infty$ strip of the honeycomb lattice is not critical at $T = 0$. This is reflected in the fact that \mathcal{B}_q only crosses the positive real axis at $q = 2$. For $q \neq 2$, the low-temperature behavior of the specific heat is given by $C \sim \text{const.} \times a$ as $a \rightarrow 0$, while for $q = 2$, $C \sim \text{const.} \times a^2$ as $a \rightarrow 0$, as follows from the equivalence and eq. (4.5). A plot of the specific heat for this antiferromagnetic case is given in Fig. 7.

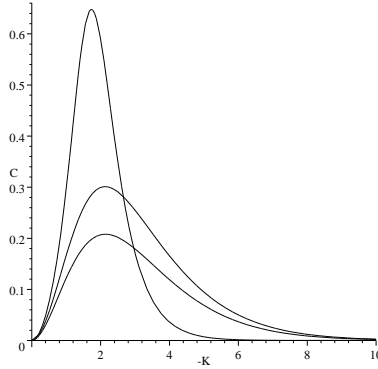


Figure 7: Specific heat C/k_B for the q -state Potts antiferromagnet on the $2 \times \infty$ strip of the honeycomb lattice as a function of $-K = -J/(k_B T) > 0$. From top to bottom, the curves are for $q = 2, 3, 4$.

5 Potts Model Partition Function for Cyclic and Möbius $L_y = 2$ Strips of the Honeycomb Lattice

5.1 Results for Z

For the cyclic and Möbius $L_y = 2$ strips of the honeycomb lattice of length m bricks $(G_s)_m = L_m, ML_m$, using the same methods as we did for the open strip discussed above, we calculate the partition functions

$$Z((G_s)_m, q, v) = \sum_{j=1}^6 c_{Z, G_s, j} (\lambda_{Z, G_s, j}(q, v))^m \quad \text{for } G_s = L, ML \quad (5.1.1)$$

where

$$\lambda_{Z, L, j} = \lambda_{Z, ML, j}, j = 1, \dots, 6 \quad (5.1.2)$$

$$\lambda_{Z, L, 1} = v^4 \quad (5.1.3)$$

$$\lambda_{Z, L, 2} = v^2(q + v)^2 \quad (5.1.4)$$

$$\lambda_{Z,L,(3,4)} = \frac{v^2}{2} \left[q^2 + 4qv + 6v^2 + v^3 \pm \sqrt{R_{34}} \right] \quad (5.1.5)$$

with

$$R_{34} = 40qv^3 + 24q^2v^2 + 8q^3v - 2q^2v^3 + 8v^5 + 32v^4 + q^4 + v^6 \quad (5.1.6)$$

and

$$\lambda_{Z,L,5} = \lambda_{Z,S,1} , \quad \lambda_{Z,L,6} = \lambda_{Z,S,2} . \quad (5.1.7)$$

For the cyclic strip the coefficients in eq. (5.1.1) are

$$c_{Z,L,1} = c^{(2)} = q^2 - 3q + 1 \quad (5.1.8)$$

$$c_{Z,L,j} = c^{(1)} = q - 1 \quad \text{for } j = 2, 3, 4 \quad (5.1.9)$$

$$c_{Z,L,j} = c^{(0)} = 1 \quad \text{for } j = 5, 6 . \quad (5.1.10)$$

For the Möbius strip,

$$c_{Z,ML,1} = -c^{(0)} = -1 \quad (5.1.11)$$

$$c_{Z,ML,2} = -c^{(1)} \quad (5.1.12)$$

$$c_{Z,ML,j} = c^{(1)} \quad \text{for } j = 3, 4 \quad (5.1.13)$$

$$c_{Z,ML,j} = 1 \quad \text{for } j = 5, 6 . \quad (5.1.14)$$

These are the same respective coefficient functions that we found for q -state Potts model partition function for the width $L_y = 2$ cyclic and Möbius strips of the square lattice and for the cyclic strip of the triangular lattice (for the Möbius strip of the triangular lattice, the coefficients are algebraic rather than polynomial functions of q) [13, 14, 16]. The respective sums of the coefficients are

$$C_{Z,L} = q^2 \quad (5.1.15)$$

and

$$C_{Z,ML} = q . \quad (5.1.16)$$

In the $T = 0$ (i.e., $v = -1$) case for the Potts antiferromagnet, where the partition function reduces to the chromatic polynomial, two of the six $\lambda_{Z,L,j}$'s vanish and the others reduce to those for the $L_y = 2$ cyclic/Möbius strip given in [38] and above:

$$\lambda_{Z,L,1} = \lambda_{P,L,1} \quad \text{for } v = -1 \quad (5.1.17)$$

$$\lambda_{Z,L,2} = \lambda_{P,L,2} = (q - 1)^2 \quad \text{for } v = -1 \quad (5.1.18)$$

$$\lambda_{Z,L,3} = \lambda_{P,L,3} = q^2 - 4q + 5 \quad \text{for } v = -1 \quad (5.1.19)$$

$$\lambda_{Z,L,j} = 0 \quad \text{for } v = -1 \quad \text{and } j = 4, 6 \quad (5.1.20)$$

$$\lambda_{Z,L,5} = \lambda_{P,L,4} = D_6 = q^4 - 5q^3 + 10q^2 - 10q + 5 \quad \text{for } v = -1 . \quad (5.1.21)$$

Here the sums of the corresponding coefficients are

$$C_{P,L} = q(q - 1) \quad (5.1.22)$$

and

$$C_{P,ML} = 0 . \quad (5.1.23)$$

For infinite temperature, $v = 0$, we have

$$\lambda_{Z,L,5} = q^4 \quad \text{for } v = 0 \quad (5.1.24)$$

$$\lambda_{Z,L,j} = 0 \quad \text{for } v = 0 \quad \text{and } j = 1, 2, 3, 4, 6 \quad (5.1.25)$$

so that the partition function reduces to

$$Z(L_m, q, 0) = Z(ML_m, q, 0) = (\lambda_{Z,L,5})^m = q^{4m} = q^n . \quad (5.1.26)$$

From our exact calculations, it follows that in the full \mathbb{C}^2 space spanned by (q, v) ,

$$\mathcal{B}(\{L\}) = \mathcal{B}(\{ML\}) . \quad (5.1.27)$$

This is the same result that we obtained for the analogous strips of other lattices [13, 14, 16, 17] and is in accord with the conclusion that the singular locus is the same for an infinite-length finite-width strip graph for given transverse boundary conditions, independent of whether the longitudinal boundary condition is cyclic or Möbius. For \mathcal{B}_q we have proved this in [48] by the use of crossing-subgraph strips, which subsume cyclic and Möbius strips as special cases (see further below). (Of course, the locus \mathcal{B} is different if one uses open, as contrasted with cyclic/Möbius, longitudinal boundary conditions.) Owing to the equality (5.1.27), we shall henceforth, for brevity of notation, refer to both $\mathcal{B}(\{L\})$ and $\mathcal{B}(\{ML\})$ as $\mathcal{B}(\{L\})$ and similarly for specific points on \mathcal{B} , such as $q_c(\{L\}) = q_c(\{ML\})$, etc.

5.2 \mathcal{B} in the q Plane

The locus \mathcal{B} exhibits a number of qualitative features similar to those that we have discussed in earlier works [13, 14, 16, 17]. Let us first consider the slice of this locus in the q plane, \mathcal{B}_q as a function of v , or equivalently, $a = v + 1$. As a increases from 0, the single crossing of \mathcal{B}_q which had been at $q = 2$ for $a = 0$ splits into two crossings. At the larger one, the boundary is determined by the equation of the degeneracy of magnitudes of leading terms $|\lambda_{Z,L,5}| = |\lambda_{Z,L,2}|$, which yields the value of q_c as the real solution of the cubic equation $q^3 + 3vq^2 + v^2(2-v)q + 2v^3 = 0$. The second crossing is determined by the equation of degeneracy of magnitudes of $|\lambda_{Z,L,j}|$ for $j = 1, 2, 4, 6$ and occurs, for $0 \leq a \leq 1$, at

$$q_{inner} = -2v = 2(1 - a) . \quad (5.2.1)$$

or equivalently, $a = -(q_{inner} - 2)/2$. Parenthetically, we note that this is the value for q_c , as a function of a , for the infinite-length limit of the circuit graph [51, 14]. In the interval $0 < q < q_{inner}$, $\lambda_{Z,L,3}$ is dominant, and, as was the case at $a = 0$, the crossing of \mathcal{B}_q at $q = 0$ is determined by the equation of degeneracy of leading terms $|\lambda_{Z,L,5}| = |\lambda_{Z,L,3}|$. For sufficiently small a near 0, there is also a pair of complex-conjugate regions where $\lambda_{Z,L,1}$ is dominant. The outermost portion of \mathcal{B}_q crosses the real axis at $q = q_c$ and $q = 0$; outside of this is the region R_1 , including the real intervals $q > q_c$ and $q < 0$. As illustrations, we show \mathcal{B}_q in Figs. 8-10 for $a = 0.1, 0.5$, and 0.9 , respectively. For the case $a = 0.9$ we note that (a) the boundary includes cusp-like structures at q_c and q_{inner} , and (b) in the pair of small complex-conjugate regions to the upper and lower right of q_{inner} , $\lambda_{Z,L,5}$ are dominant. In general, as the temperature T increases from 0 to infinity for the Potts antiferromagnet, i.e. as a increases from 0 to 1, the locus \mathcal{B} moves in toward the origin in the q plane and degenerates to a point at the origin for $a = 1$.

The boundary \mathcal{B}_q for the Potts ferromagnet is given for the illustrative finite-temperature value $a = 2$ in Fig. 11. Compared with analogous figures for the infinite-length limits of the $L_y = 2$ strips of the square

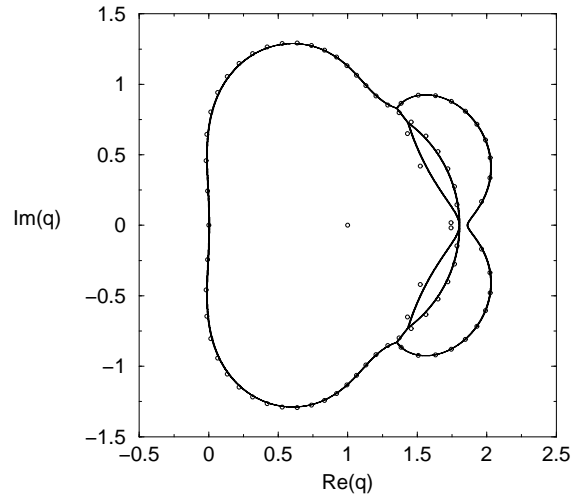


Figure 8: Locus $\mathcal{B}_q(\{L\})$ for the Potts antiferromagnet on the $m \rightarrow \infty$ limit of the cyclic or Möbius $L_y = 2$ strip of the honeycomb lattice for $a = 0.1$. For comparison, chromatic zeros are shown for the cyclic strip with $m = 20$ (i.e., $n = 80$).

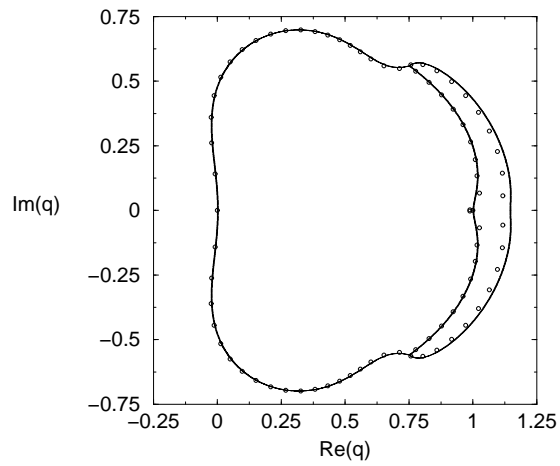


Figure 9: Same as Fig. 8, for $a = 0.5$.

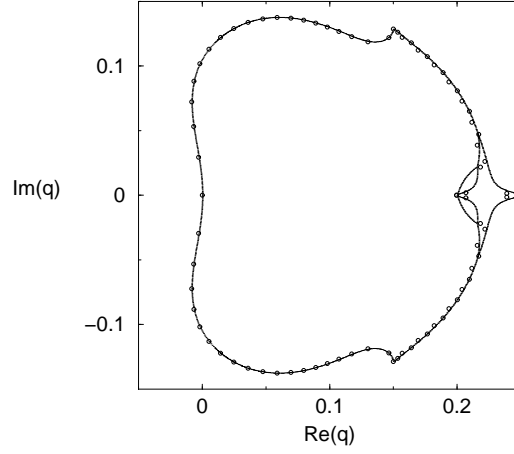


Figure 10: Same as Fig. 8, for $a = 0.9$.

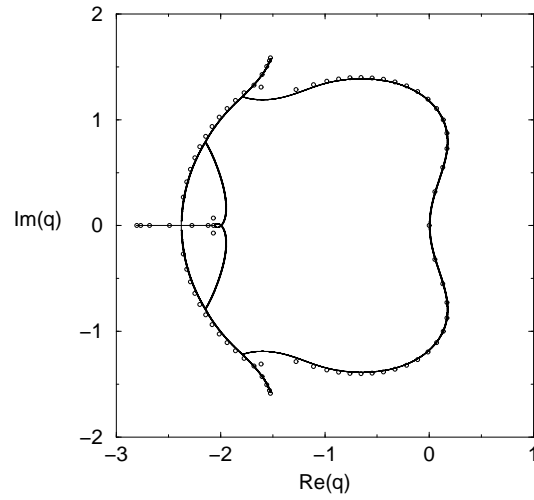


Figure 11: Locus $\mathcal{B}_q(\{L\})$ for the Potts ferromagnet on the $m \rightarrow \infty$ limit of the cyclic or Möbius $L_y = 2$ strip of the honeycomb lattice for $a = 2$. For comparison, chromatic zeros are shown for the cyclic strip with $m = 20$ (i.e., $n = 80$).

and triangular lattices (Figs. 13 in [14] and [16]), one sees the common feature that \mathcal{B}_q passes through $q = 0$, does not cross the positive real q , but does have complex-conjugate lobes that extend into the $\text{Re}(q) > 0$ half-plane. Similar to \mathcal{B}_q for this strip of the square lattice, here \mathcal{B}_q contains a finite line-segment on the negative q axis, whereas such a line segment is not present on \mathcal{B}_q for the triangular strip for this value of a .

5.3 \mathcal{B} in the Complex-Temperature Plane

We next discuss slices of \mathcal{B} in the complex-temperature plane, as a function of q . In Figs. 12-17 we show plots of \mathcal{B} for $q = 2, 3, 4$, and 10. The locus \mathcal{B} is noncompact in the a plane and, for $q \neq 2$, compact in the u plane. For $q = 2$ there can be noncommutativity of the type (1.9); the results that we show are for the f_{nq} definition, i.e., we set $q = 2$ first before taking the limit $n \rightarrow \infty$. For comparison with previous calculations of complex-temperature zeros in [57, 62], we show some plots in the a plane as well as u plane.

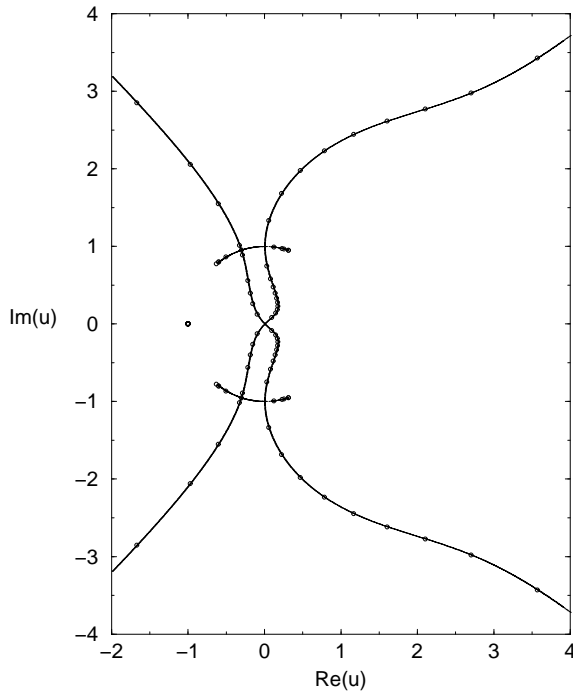


Figure 12: Locus $\mathcal{B}_u(\{L\})$ for the $m \rightarrow \infty$ limit of the cyclic strip of the honeycomb lattice with $q = 2$. Partition function zeros are shown for $m = 20$, so that Z is a polynomial of degree $e = 5m = 100$ in v and hence, up to an overall factor, in u .

In the u plane, four curves forming two branches of \mathcal{B} cross at $u = 0$, reflecting the $T = 0$ critical point of the q -state Potts ferromagnet. In general, the density of complex-temperature (i.e., Fisher [58]) zeros along the curves comprising \mathcal{B} in the vicinity of a generic singular point u_s behaves as [59]

$$g \sim |u - u_s|^{1-\alpha_s} \quad (5.3.1)$$

where α_s (α'_s) denotes the corresponding specific heat exponent for the approach to u_s from within the CTE PM (FM) phase. Thus, for a continuous, second-order transition, with $\alpha_s < 1$, this density vanishes as one approaches the critical point u_s along \mathcal{B} , while, in contrast, if $\alpha_s = 1$, corresponding to a first-order transition, this density would remain nonzero as the boundary crosses u_s , and there would be a discontinuity

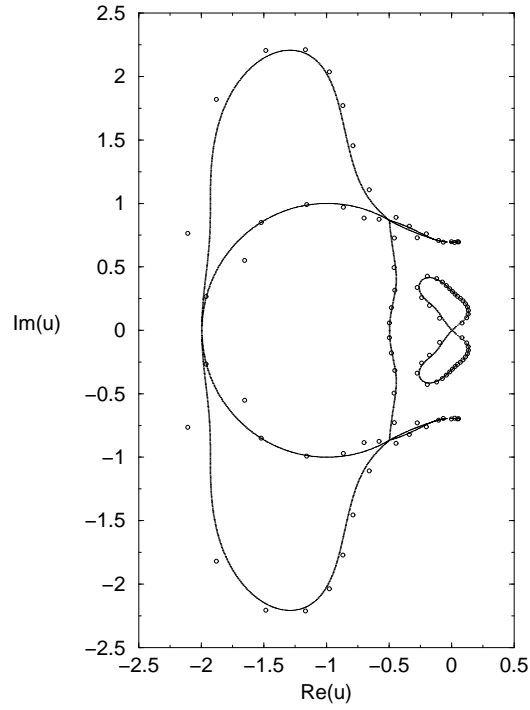


Figure 13: Locus $\mathcal{B}_u(\{L\})$ for $q = 3$. Partition function zeros are shown for $e = 100$, as in Fig. 12.

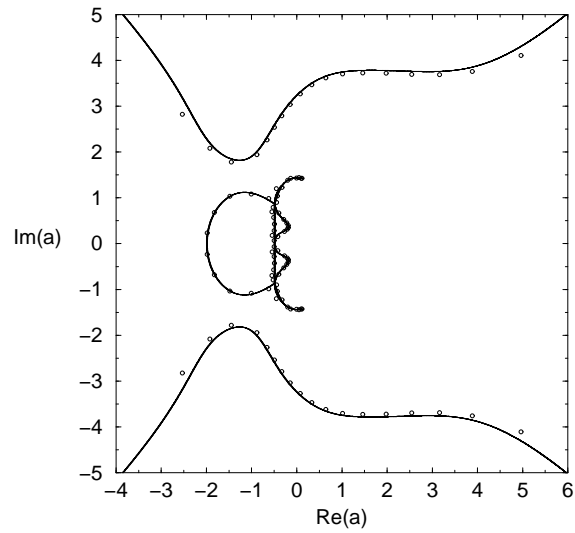


Figure 14: Locus $\mathcal{B}_a(\{L\})$ for $q = 3$. Partition function zeros are shown for $e = 100$.

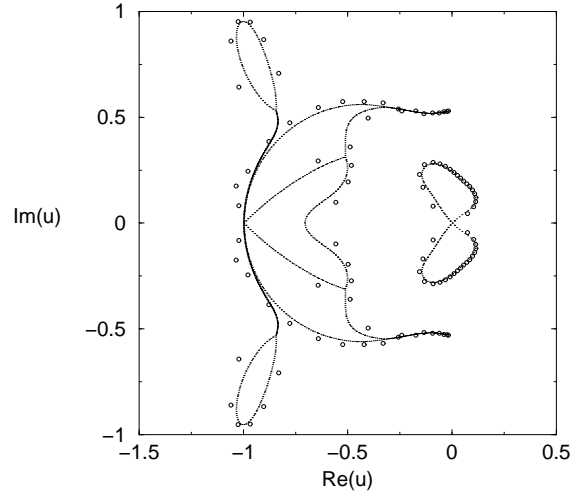


Figure 15: Locus $\mathcal{B}_u(\{L\})$ for $q = 4$. Partition function zeros are shown for $e = 100$.

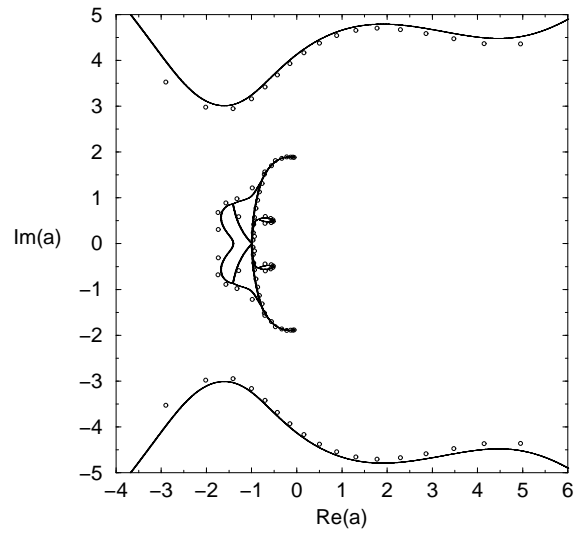


Figure 16: Locus $\mathcal{B}_a(\{L\})$ for $q = 4$. Partition function zeros are shown for $e = 100$.

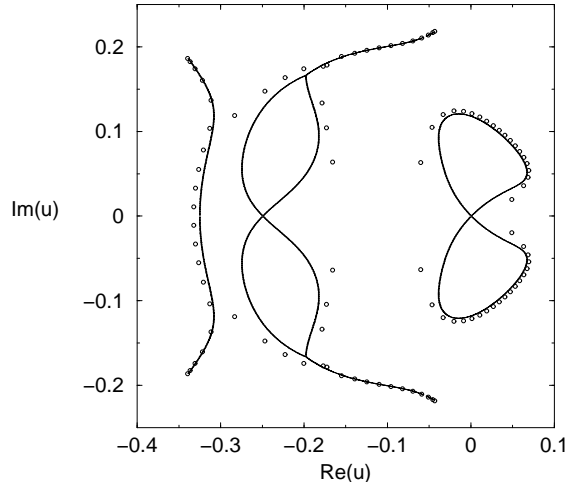


Figure 17: Locus $\mathcal{B}_u(\{L\})$ for $q = 10$. Partition function zeros are shown for $e = 100$.

in the internal energy, U . (We recall that this is analogous to the discontinuity in $M(H)$ for $T < T_c$ as one changes H from positive through zero to negative values, and the connection to the nonzero density of Yang-Lee (complex-field) zeros, via the relation $M(T) = 2\pi g(H = 0)$, where $M(T)$ is the spontaneous magnetization [60, 61].) Now the essential zero in the specific heat in (4.5) at $T = 0$, if expressed in terms of an algebraic specific exponent α , corresponds to $\alpha = -\infty$ at $u = u_s = 0$. Substituting this into (5.3.1), it follows that the density vanishes rapidly as one approaches the origin $u = 0$ along the curves forming \mathcal{B}_u . This is evident in Figs. 12 and 13. The angles at which these curves cross the origin are $\pm\pi/4$ and $\pm3\pi/4$, as is clear in both of the figures shown, for $q = 2$ and 3. In particular, in the Ising case $q = 2$, because of the bipartite property of the cyclic strip of the honeycomb lattice, the antiferromagnetic and ferromagnetic versions of the model are equivalent, and so the antiferromagnet also has a $T = 0$ critical point. This is manifested in the fact that \mathcal{B}_a passes through the origin of the a plane and \mathcal{B}_q passes through the point $q = 2$. Indeed, for this value $q = 2$, the locus \mathcal{B} is the same in the a and u plane, i.e. it is invariant under the inversion map $a \rightarrow a^{-1} = u$. As was the case with the phase diagram for the infinite-length limit of the open strip, the positive u axis and its maximal complex-temperature analytic continuation forms the (CTE)PM phase. As discussed earlier [13, 14, 46], the fact that, for $a = 0$, the crossing of \mathcal{B}_q at $q = 2$ signals the property that the Ising antiferromagnet on the finite-width, infinite-length strips of the square lattice has a $T = 0$ critical point is a useful feature of the periodic or reversed-orientation periodic longitudinal boundary conditions; in contrast, the loci \mathcal{B}_q at $a = 0$ for strips with free longitudinal boundary conditions do not, in general, pass through $q = 2$. Furthermore, just as we showed by exact calculations in the case with the strips of the square lattice, in the present case of the honeycomb lattice, we anticipate that at the antiferromagnetic zero-temperature value $a = 0$, i.e., $v = -1$, the loci \mathcal{B}_q for wider cyclic/Möbius strips will

exhibit at least three crossings: (i) at a value q_c that approaches the value for the infinite honeycomb lattice

$$q_c(hc) = \frac{3 + \sqrt{5}}{2} = 2.61803... \quad (5.3.2)$$

(the relevant root of eq. (5.3.3) for $v = -1$, as discussed below), (ii) at $q = 2$, reflecting the $T = 0$ critical point of the Ising antiferromagnet on these strips, and (iii) at $q = 0$.

One of the reasons for interest in the complex-temperature phase diagrams for the q -state Potts model on infinite-length, finite-width strips of various lattices is that these provide exact results that exhibit features which can give insight into the properties of the complex-temperature phase diagrams of the corresponding Potts model on the respective 2D lattices [14, 16]. Of course for the $q = 2$ Ising case, since the model is solved, this complex-temperature phase diagram is known [50]. However, for other values of q , these insights can help one in interpreting the information that one has from calculations of complex-temperature zeros on finite sections of the honeycomb lattice [57, 62]. In order to appreciate some of the similar features in the complex-temperature phase diagrams, we recall that \mathcal{B}_a for the Ising model on the honeycomb lattice consists of an arc of the unit circle $a = e^{\pm i\theta}$ with $\pi/3 \leq \theta \leq \pi$, together with a closed, bean-shaped curve that intersects the real axis at $a = 2 - \sqrt{3}$, the paramagnetic-antiferromagnetic critical point, and its inverse, $a = 2 + \sqrt{3}$, the paramagnetic-ferromagnetic critical point [50]. The arc of the unit circle and the closed curve intersect at $a = \pm i$. There are, of course, obvious qualitative differences between the locus \mathcal{B}_a for the finite-width, infinite-length strip and the full 2D honeycomb lattice, reflecting the fact that the 2D Ising ferromagnetic (and equivalently, the antiferromagnet) has a finite-temperature critical point, while this occurs only at zero-temperature on the infinite-length, finite-width strip, which is effectively a quasi-one-dimensional system. However, for both the strip and the full honeycomb lattice, \mathcal{B}_a includes intersection points where two branches of curves cross at $a = \pm i$. The locus \mathcal{B}_a for the infinite-length $L_y = 2$ strip also exhibits complex-conjugate arc endpoints in the $Re(a) > 0$ half-plane, as is true of the exactly solved Ising model on the full 2D honeycomb lattice; in addition, this locus for the strip exhibits complex-conjugate arc endpoints in the $Re(a) < 0$ half-plane. This illustrates how, although physical temperature properties of the Potts model on an finite-width, infinite strip of a given lattice and on the full 2D lattice are clearly different, complex-temperature properties can have some similarities.

Having discussed the situation with the $q = 2$ case, where the 2D model is exactly solved, let us proceed to cases where the 2D Potts model has not been solved. In general, for the honeycomb lattice, from duality and a star-triangle relation, one can derive an algebraic equation for the PM-FM and PM-AFM critical points [2, 52, 53]

$$v^3 - 3qv - q^2 = 0. \quad (5.3.3)$$

(where $v = a - 1$). For example, for $q = 3$, the equation yields three solutions (tabulated, e.g., as eqs. (3.3)-(3.5) in [57]), namely (i) the PM-FM critical point at $a_{PM-FM,q=3} = 1 + 2\sqrt{3}\cos(\pi/18) = 4.41147...$, and two complex-temperature singular points, at $a = 1 - \sqrt{3}\cos(\pi/18) + 3\sin(\pi/18) = -0.1847925...$ and $a = 1 - \sqrt{3}\cos(\pi/18) - 3\sin(\pi/18) = -1.22668...$. There is no physical PM-AFM critical point solution, and the absence of such a phase transition was confirmed by explicit Monte Carlo study of the model in [54] (and further confirmed in [55]). More generally, considering this solution as a function of q generalized from positive integer to real values, one sees that it decreases from the $q = 2$ Ising value $a = \sqrt{2} - 1$ and passes through $a = 0$ at the value $q_c(hc)$ given in eq. (5.3.2) above (see the middle curve in Fig. 4 of [57]), corresponding to a zero-temperature critical point for the Potts antiferromagnet at this value of q . For $q_c(hc) \leq q \leq 4$, this root decreases from 0 to -1 , where it coalesces with another solution (the lower curve in

Fig. 4 of [57]) to form a double root, and for $q > 4$, eq. (5.3.3) has only a single real root, namely the PM-FM critical point. In [56], as a rigorous result of duality, it was shown that as a consequence of the (first-order) phase transition of the $q = 3$ Potts antiferromagnet on the triangular lattice at $a_{PM-FM,t} \simeq 0.203$, it follows that for $q = 3$ Potts model on the honeycomb lattice, the left-most crossing of the locus \mathcal{B}_a is at the complex-temperature point given by the duality mapping $v \rightarrow q/v$, i.e.,

$$a \rightarrow \frac{q + a - 1}{a - 1} \quad (5.3.4)$$

i.e., $a \simeq -2.76$. The calculations of complex-temperature zeros in [57] (given in Figs. 5-7 of that paper) were consistent with these crossings of \mathcal{B}_a at $a \simeq -2.76$, -1.23 , and -0.185 and also suggested a fourth possible crossing, at $a \simeq -0.65$, for a total of four crossings on the negative real a axis.

For the $q = 3$ Potts model on the infinite-length strip, as shown in Fig. 14, we find that \mathcal{B}_a crosses the negative real a axis at two points, $a = -1/2$ and $a = -2$. In order to relate this complex-temperature phase diagram to one for the $q = 3$ Potts model on the 2D honeycomb lattice, one can imagine performing a transformation in which one retracts the branches of the curves forming \mathcal{B}_a from the zero-temperature ferromagnet critical point at $u = 0$; in the right-hand half-plane, one would then reconnect the two branches of the curve so as to cross the positive real a axis at the value of $a_{PM-FM,q=3}$ given above, while in the left-hand half plane, one would reconnect the branches to cross at a point on the negative real a axis. One could also pull apart the two curves that have a tacnode multiple point at $a = -1/2$ to obtain a total of four crossings on the negative real axis, as appears to be the case for the model on the full 2D honeycomb lattice. The exactly determined locus \mathcal{B}_a also exhibits a complex-conjugate pair of arc endpoints in the $Re(a) > 0$ half-plane, qualitatively similar to the arc endpoints that appear to be formed by the complex-temperature zeros for 2D honeycomb lattice. Thus, although the physical thermodynamic properties are clearly different, certain complex-temperature features of the phase diagram for the $q = 3$ Potts model on the infinite-length, width $L_y = 2$ strip of the honeycomb lattice show interesting qualitative similarities to those inferred for the complex-temperature phase diagram of the model on the full honeycomb lattice.

We next consider the case $q = 4$. For this value, eq. (5.3.3) reduces, in terms of the variable a , to $(a - 5)(a + 1)^2 = 0$, yielding the physical PM-FM critical point $a_{PM-FM,q=4} = 5$ and a double root at the complex-temperature point $a = u = -1$. As in the $q = 3$ case, there is no phase transition at finite or zero temperature for the $q = 4$ Potts antiferromagnet. From the duality relation given in [56] together with the fact that the $q = 4$ Potts antiferromagnet has a $T = 0$ critical point on the triangular lattice, it follows that the left-most crossing of \mathcal{B}_a on the real axis for the $q = 4$ Potts model on the honeycomb lattice is at the value of a given by (5.3.4), viz., $a = -3$. The calculations of complex-temperature zeros in [62] (see Figs. 2-4 of that paper) exhibited these three crossings of the complex-temperature phase boundary \mathcal{B}_a at $a = 5$, $a = -1$ and $a = -3$ and also suggested crossings at approximately $a = -2$ and $a = -1/2$. The locus \mathcal{B}_a also exhibited a pair of arc endpoints (prongs) in the $Re(a) > 0$ half-plane and structures that resembled a complex-conjugate pair of prongs or bulbs in the $Re(a) < 0$ half-plane, all within the interior of the PM phase.

What insights can we draw for this $q = 4$ case from our exact results for the infinite-length, $L_y = 2$ strip? The locus \mathcal{B} is shown in the u and a planes in Figs. 15 and 16. In the a plane, we again perform a transformation to remove the intrinsically 1D features of the complex-temperature phase boundary, i.e. their passage through $u = 0$ for the comparison with the 2D results. We thus retract the branches of the curves passing through this point; in the right-hand half-plane, we reconnect the two branches of the curve so as to cross the positive real a axis at the value of $a_{PM-FM,q=4}$ given above, while in the left-hand half plane,

we reconnect the branches to cross at a point on the negative real a axis, which then forms the left-most crossing. We could also pull apart the curves that meet and cross at $a = -1$, thereby obtaining four crossings of \mathcal{B}_a on the negative real a axis. The two complex-conjugate pairs of arc endpoints on \mathcal{B}_a are in nice 1-1 correspondence with those observed for the model on the 2D honeycomb lattice in [62]. In addition, \mathcal{B}_a exhibits two small bulb-like structures around $a = -0.65 \pm 0.53i$; these bear an interesting correspondence to the analogous structures found in [62]. This discussion shows how some qualitative aspects of the complex-temperature phase diagram for the Potts model on the 2D honeycomb lattice can correspond to those found via exact solutions for infinite-length, finite-width strips. One of the most remarkable findings is that the crossing point of \mathcal{B}_a at $a = u = -1$ for the infinite-length strip is not just qualitatively but exactly the same as one finds, rigorously, from the solution of (5.3.3), for \mathcal{B}_a on the infinite honeycomb lattice. This is also true for the infinite triangular lattice [62], since it is dual to the honeycomb lattice, and under the duality mapping (5.3.4), $a = -1$ maps to itself if $q = 4$. As was discussed in [65], the point $a = -1$ is a solution of the equation for the critical manifold, $v^2 = q$, at $q = 4$ and hence \mathcal{B}_a passes through $a = -1$ for the square lattice. Calculations of complex-temperature zeros for the $q = 4$ Potts model on large finite sections of the triangular lattice in [62] and the square lattice (see [64, 63, 65] and references therein) are both consistent with these exact results. Moreover, our exact determinations of \mathcal{B}_a for the 1D Potts model (i.e., $n \rightarrow \infty$ limit of the circuit graph) [51, 14] and infinite-length, $L_y = 2$ cyclic/Möbius and open strips of the square and triangular lattices [14, 16] showed that in all cases, if $q = 4$, then \mathcal{B}_a passes through $a = -1$. It is of interest to see what the values $q = 4$, $a = v + 1 = -1$ correspond to in terms of the variables x and y , defined in eqs. (13.2.3) and (13.2.4), that enter in the Tutte polynomial equivalent to the Potts model partition function (see eqs. (13.2.1) and (13.2.6)). We find that $(q, v) = (4, -2)$ corresponds to the symmetric point $(x, y) = (-1, -1)$. More generally, one can investigate the continuous accumulation set of zeros of the Tutte polynomial in the complex x plane for fixed y , \mathcal{B}_x and in the complex y plane for fixed x , \mathcal{B}_y . Since this information is equivalent to our study of the loci \mathcal{B}_q for fixed u and \mathcal{B}_u for fixed q , we shall not include the results here.

An illustration of \mathcal{B}_u for larger values of q is given for the case $q = 10$ in Fig. 17. This locus includes two separate figure-eight type curves, the one to the left also involving outgoing arcs, and, to the far left, a self-conjugate arc. As compared with our result for the infinite-length $L_y = 2$ strip of the square lattice in Fig. 17 of [14], one sees that the middle figure-eight curve plus outlying arcs that are present on \mathcal{B}_u for the honeycomb strip are absent in the locus for the strip of the square lattice, while the other two components (the self-conjugate arc on the left and the figure-eight curve on the right) are qualitatively similar. For the infinite-length honeycomb lattice strip with open boundary conditions, we note that \mathcal{B}_u consists of the same self-conjugate arc on the left as in Fig. 17, together with two complex-conjugate pairs of arcs.

6 $L_y = 3$ Cyclic and Möbius Strips of the Honeycomb Lattice

Illustrations of strips of the honeycomb lattice with width $L_y = 3$ and $(FBC_y, PBC_x) =$ cyclic and $(FBC_y, TPBC_x) =$ Möbius boundary conditions, displayed as strips of a brick lattice, are shown in Fig. 18 (a,b).

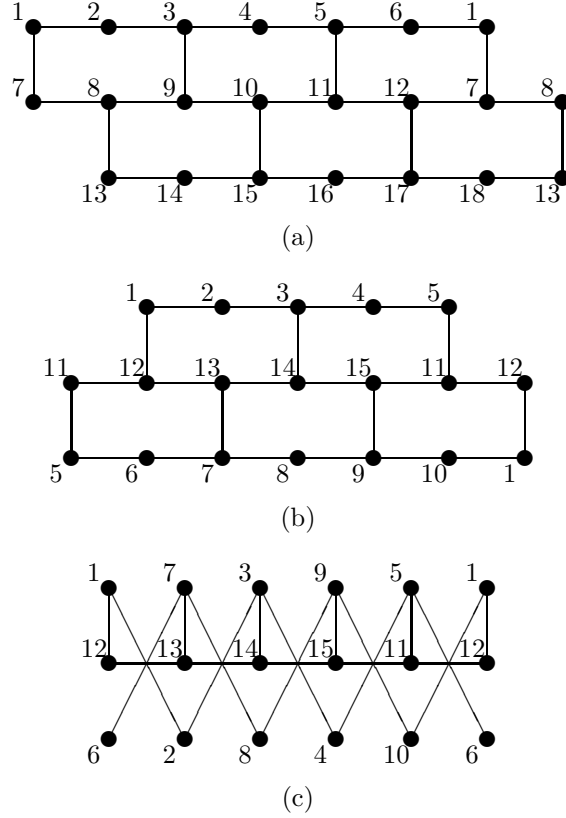


Figure 18: Illustrative strip graphs of the honeycomb lattice, displayed as a brick lattice, with width $L_y = 3$: (a) cyclic, length $m = 3$ and (b) Möbius, length $m = 2$. We also show (c) an $L_y = 3$ cyclic crossing-subgraph strip of the honeycomb lattice with length $\ell = 5$. As discussed in the text, the cyclic crossing-subgraph strips of a given width are equivalent to the cyclic and Möbius strips of the same width for even and odd ℓ , respectively. This equivalence is illustrated here; graph (c) is equivalent to (b).

We calculate the chromatic polynomials by iterated use of the deletion-contraction theorem and by coloring matrix methods. Here and below, in our results for chromatic polynomials, we shall suppress the subscript P in $\lambda_{P,G,j}$ and $c_{P,G,j}$ where it is obvious. For the $L_y = 3$ cyclic and Möbius strips of the honeycomb lattice, denoted $hc3c = hc, 3 \times m, FBC_y, PBC_x$ and $hc3mb = hc, 3 \times m, FBC_y, TPBC_x$, we obtain the result $N_{hc3c,\lambda} = N_{hc3mb,\lambda} = 14$ and

$$P(hc, 3 \times m, FBC_y, PBC_x, q) = \sum_{j=1}^{14} c_{hc3c,j} (\lambda_{hc3,j})^m \quad (6.1)$$

$$P(hc, 3 \times m, FBC_y, TPBC_x, q) = \sum_{j=1}^{14} c_{hc3mb,j} (\lambda_{hc3,j})^m \quad (6.2)$$

where, for $j = 1, 2$,

$$\lambda_{hc3,1} = 1 \quad (6.3)$$

and

$$\lambda_{hc3,2} = (q - 1)^2. \quad (6.4)$$

Note that

$$\lambda_{hc3,j} = \lambda_{hc2,j} \quad \text{for } j = 1, 2. \quad (6.5)$$

The $\lambda_{hc3,j}$ for $j = 3, 4, 5$ are the roots of the cubic equation

$$\xi^3 - (2q^2 - 8q + 11)\xi^2 + (q^4 - 8q^3 + 26q^2 - 38q + 23)\xi - (q - 1)^2 = 0 \quad (6.6)$$

and the $\lambda_{hc3,j}$ for $6 \leq j \leq 11$ are the roots of the sixth degree equation

$$\begin{aligned} & \xi^6 - (3q^4 - 18q^3 + 46q^2 - 60q + 37)\xi^5 \\ & + (3q^8 - 36q^7 + 199q^6 - 662q^5 + 1456q^4 - 2172q^3 + 2144q^2 - 1278q + 358)\xi^4 \\ & - (q^{12} - 18q^{11} + 154q^{10} - 828q^9 + 3117q^8 - 8646q^7 + 18070q^6 - 28564q^5 + 33782q^4 \\ & - 29110q^3 + 17370q^2 - 6466q + 1142)\xi^3 \\ & (q - 1)^2(q^{12} - 20q^{11} + 186q^{10} - 1060q^9 + 4115q^8 - 11454q^7 + 23448q^6 \\ & - 35642q^5 + 40094q^4 - 32780q^3 + 18680q^2 - 6756q + 1197)\xi^2 \\ & - (q - 1)^4(2q^8 - 26q^7 + 150q^6 - 498q^5 + 1037q^4 - 1388q^3 + 1176q^2 - 590q + 141)\xi \\ & + (q - 2)^2(q - 1)^8 = 0 . \end{aligned} \quad (6.7)$$

Finally, $\lambda_{hc3,j}$ for $12 \leq j \leq 14$ are roots of the cubic equation

$$\begin{aligned} & \xi^3 - (q^6 - 8q^5 + 28q^4 - 56q^3 + 71q^2 - 58q + 26)\xi^2 \\ & + (q - 1)^2(q^6 - 10q^5 + 43q^4 - 102q^3 + 144q^2 - 120q + 49)\xi \\ & - (q - 2)^2(q - 1)^4 = 0 . \end{aligned} \quad (6.8)$$

The corresponding coefficients for the cyclic strip are

$$c_{hc3c,1} = c^{(3)} \quad (6.9)$$

$$c_{hc3c,j} = c^{(2)} \quad \text{for } 2 \leq j \leq 5 \quad (6.10)$$

$$c_{hc3c,j} = c^{(1)} \quad \text{for } 6 \leq j \leq 11 \quad (6.11)$$

$$c_{hc3c,j} = c^{(0)} = 1 \quad \text{for } 12 \leq j \leq 14 . \quad (6.12)$$

For the Möbius strip, as will be discussed further below in section 7, the coefficients are not, in general, simply ± 1 times Chebyshev polynomials of the second kind, $c^{(d)}$, but instead are products of the $c^{(d)}$ with certain terms $\lambda_{cghc3,j}$'s occurring in the chromatic polynomial for related families of strip graphs called crossing-subgraph strips, defined via eqs. (7.2)-(7.8). We have

$$c_{hc3mb,1} = -c^{(2)} = -(q^2 - 3q + 1) \quad (6.13)$$

$$c_{hc3mb,2} = -c^{(0)}\lambda_{cghc3,3} = -(q - 1) \quad (6.14)$$

$$c_{hc3mb,j} = -c^{(0)}\lambda_{cghc3,j+2} \quad \text{for } j = 3, 4, 5 \quad (6.15)$$

$$c_{hc3mb,j} = c^{(1)}\lambda_{cghc3,j+5} \quad \text{for } 6 \leq j \leq 11 \quad (6.16)$$

$$c_{hc3mb,j} = c^{(0)}\lambda_{cghc3,j+5} \quad \text{for } 12 \leq j \leq 14 . \quad (6.17)$$

By general coloring matrix methods, we have

$$C_{P,G} = q\left(q(q-1)\right)^{\frac{L_y-1}{2}} \quad \text{for } G = hc, L_y \times m, FBC_y, PBC_x, L_y \text{ odd} \quad (6.18)$$

$$C_{P,G} = \left(q(q-1)\right)^{\frac{L_y}{2}} \quad \text{for } G = hc, L_y \times m, FBC_y, PBC_x, L_y \text{ even} \quad (6.19)$$

Our results for the Möbius strips lead to the inference that

$$C_{P,G} = 0 \quad \text{for } G = hc, L_y \times m, FBC_y, TPBC_x . \quad (6.20)$$

The first special case of this, for $L_y = 2$, was obtained in [38].

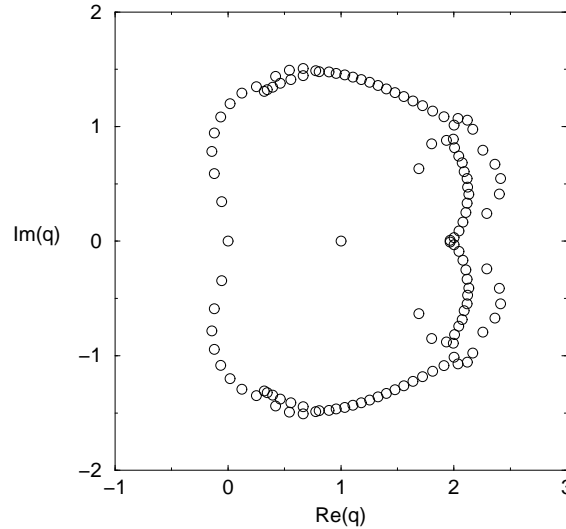


Figure 19: Chromatic zeros for the $L_y = 3$ cyclic strip of the honeycomb lattice of length $m = 20$, i.e., $n = 120$ vertices.

As a special case of the arguments given in [43], since the $\lambda_{G,j}$'s are the same for the cyclic and Möbius strips, and since in the limit $m \rightarrow \infty$ the continuous singular locus \mathcal{B} is defined as the solution to the degeneracy of leading terms $\lambda_{G,j}$, it follows that this locus is the same for the cyclic and Möbius strips. In Fig. 19 we show the chromatic zeros for a cyclic strip of the honeycomb lattice with width $L_y = 3$ and length, $m = 20$, i.e., $n = 120$ vertices. This length is sufficiently great that the chromatic zeros for the cyclic and Möbius strips are generally similar and lie close to the asymptotic singular locus \mathcal{B} . We find the exact result

$$q_c = 2 \quad \text{for } hc, 3 \times \infty, FBC_y, (T)PBC_x . \quad (6.21)$$

This is the same value that was obtained in [38] for the ($m \rightarrow \infty$ limit of the) $L_y = 2$ cyclic or Möbius strip of the honeycomb lattice (below we shall show that the $L_y = 4$ strip with cylindrical boundary conditions yields a value of q_c closer to the value (5.3.2) for the infinite 2D honeycomb lattice). The locus \mathcal{B} for $L_y = 3$ has support for $Re(q) < 0$ as well as $Re(q) > 0$, just as was true for $L_y = 2$ [38].

This $L_y = 3$ locus separates the q plane into several regions. The outermost one, region R_1 , extends to infinite $|q|$ and includes the intervals $q > 2$ and $q < 0$ on the real q axis. Region R_2 includes the real interval $0 < q < 2$. Two complex-conjugate regions R_3, R_3^* , centered at approximately $q = 2.25 \pm 0.55i$, occur to the upper and lower right of q_c , as is evident in Fig. 19. Two further complex-conjugate regions, R_4, R_4^* , centered at approximately $q = 1.9 \pm 0.5i$, occur to the upper and lower left of q_c . One can observe that, just as was the case for $L_y = 2$, the density of zeros is small on the boundary separating region R_4 from R_2 and its complex conjugate boundary separating R_4^* from R_2 . As previous exact calculations have shown [36, 40, 45], region diagrams for infinite-length, finite-width strips of lattices can also include extremely small regions. We have found evidence for a complex-conjugate pair of these tiny regions to the upper and lower right of q_c . We have not made an exhaustive search for other tiny regions.

In region R_1 , the dominant $\lambda_{hc3,j}$ is the root of the cubic equation (6.8) with the largest magnitude, which we denote as $\lambda_{hc3,12}$. Hence,

$$W = (\lambda_{hc3,12})^{1/6}, \quad q \in R_1. \quad (6.22)$$

The fact that this is the same as W for the (FBC_y,FBC_x) case [35] is a general result [13]. In region R_2 , and also in regions R_3, R_3^* , the dominant terms are the roots of eq. (6.7) that are largest in magnitude in these respective regions. We shall refer to these respective dominant terms generically as $\lambda_{hc3,6}$, so that

$$|W| = |\lambda_{hc3,6}|^{1/6}, \quad q \in R_2, R_3, R_3^*. \quad (6.23)$$

In regions R_4, R_4^* , the dominant term is the root of eq. (6.6) with maximal magnitude, which we denote as $\lambda_{hc3,3}$, so that

$$|W| = |\lambda_{hc3,3}|^{1/6}, \quad q \in R_4, R_4^*. \quad (6.24)$$

Note that $W = 1$ at $q_c = 2$. A summary of some features of these strip graphs is given in Table 1. Regarding the comparison with previous results, those for the $L_y = 2$ cyclic/Möbius strips are from Ref. [38] and those for the $L_y = 3$ open strip are from Ref. [35].

7 $L_y = 3$ Cyclic Crossing-Subgraph Strips of the Honeycomb Lattice

An illustration of the cyclic $L_y = 3$ crossing-subgraph strip of the honeycomb lattice, denoted $cghc3$, of length $\ell = 5$, is shown in Fig. 18 (c). For this type of strip, with arbitrarily great ℓ , we calculate $N_{cghc3,cyc.} = 19$ and

$$P(cghc, 3 \times \ell, FBC_y, PBC_x, q) = \sum_{j=1}^{19} c_{cghc3,j} (\lambda_{cghc3,j})^\ell \quad (7.1)$$

where for $1 \leq j \leq 4$,

$$\lambda_{cghc3,1} = -\lambda_{cghc3,2} = 1 \quad (7.2)$$

$$\lambda_{cghc3,3} = -\lambda_{cghc3,4} = q - 1. \quad (7.3)$$

Table 1: Properties of P , W , and \mathcal{B} for strip graphs G_s of the honeycomb (hc) lattice. The properties apply for a given strip of size $L_y \times m$; some apply for arbitrary m , such as N_λ , while others apply for the infinite-length limit, such as the properties of the locus \mathcal{B} . For the boundary conditions in the y and x directions (BC_y , BC_x), F, P, and T denote free, periodic, and orientation-reversed (twisted) periodic, and the notation (T)P means that the results apply for either periodic or orientation-reversed periodic. The column denoted eqs. describes the numbers and degrees of the algebraic equations giving the $\lambda_{G_s,j}$; for example, $\{2(1), 2(3), 1(6)\}$ indicates that there are 2 linear equations, 2 cubic equations and one sixth degree equation. The column denoted BCR lists the points at which \mathcal{B} crosses the real q axis and the value of q_c for the given family. The notation “none” in this column indicates that \mathcal{B} does not cross the real q axis. The notation “int; q_1, q_c ” refers to cases where \mathcal{B} contains a real interval, there is a crossing at q_1 , and the right-hand endpoint of the interval is q_c . Column labelled “SN” refers to whether \mathcal{B} has support for negative $Re(q)$, indicated as yes (y) or no (n).

L_y	BC_y	BC_x	N_λ	eqs.	BCR	SN
2	F	F	1	$\{1(1)\}$	none	n
3	F	F	3	$\{1(3)\}$	2	n
4	F	F	5	$\{1(5)\}$	int;2.093,2.099	n
2	F	(T)P	4	$\{4(1)\}$	0, 2	y
3	F	(T)P	14	$\{2(1),2(3),1(6)\}$	0, 2	y
4	P	F	4	$\{1(4)\}$	int;2.222,2.250	y

The $\lambda_{cghc3,j}$ for $j = 5, 6, 7$ are the roots of the cubic equation

$$\xi^3 + \xi^2 - (q^2 - 4q + 5)\xi - (q - 1) = 0. \quad (7.4)$$

The $\lambda_{cghc3,j}$ for $j = 8, 9, 10$ are the roots of the cubic equation

$$\xi^3 - \xi^2 - (q^2 - 4q + 5)\xi + (q - 1) = 0. \quad (7.5)$$

Since eq. (7.5) is related to eq. (7.4) by the reversal of the signs of the coefficients of the ξ^2 and ξ^0 terms, it follows that the respective roots of these equations are opposite in sign:

$$\lambda_{cghc3,j} = -\lambda_{cghc3,j+3} \quad \text{for } j = 5, 6, 7. \quad (7.6)$$

The $\lambda_{cghc3,j}$ for $11 \leq j \leq 16$ are the roots of the sixth degree equation

$$\begin{aligned} &\xi^6 + (q^2 - 4q + 5)\xi^5 - (q^4 - 5q^3 + 10q^2 - 10q + 6)\xi^4 \\ &- (q^6 - 10q^5 + 43q^4 - 102q^3 + 142q^2 - 110q + 38)\xi^3 \\ &+ (q - 1)(q^6 - 10q^5 + 43q^4 - 100q^3 + 132q^2 - 94q + 29)\xi^2 \\ &+ (q - 1)^2(q^2 - 4q + 5)\xi - (q - 2)(q - 1)^4 = 0. \end{aligned} \quad (7.7)$$

Finally, the $\lambda_{cghc3,j}$ for $j = 17, 18, 19$ are the roots of the cubic equation

$$\xi^3 - (q - 2)(q^2 - 2q + 3)\xi^2 + (q - 1)(q^3 - 5q^2 + 8q - 5)\xi - (q - 2)(q - 1)^2 = 0. \quad (7.8)$$

The corresponding coefficients are

$$c_{cghc3,1} = \frac{1}{2}(c^{(3)} - c^{(2)}) = \frac{1}{2}(q - 2)(q^2 - 4q + 1) \quad (7.9)$$

$$c_{cghc3,2} = \frac{1}{2}(c^{(3)} + c^{(2)}) = \frac{1}{2}q(q-1)(q-3) \quad (7.10)$$

$$c_{cghc3,j} = \frac{1}{2}(c^{(2)} - c^{(0)}) = \frac{1}{2}q(q-3) \quad \text{for } j = 3, 5, 6, 7 \quad (7.11)$$

$$c_{cghc3,j} = \frac{1}{2}(c^{(2)} + c^{(0)}) = \frac{1}{2}(q-1)(q-2) \quad \text{for } j = 4, 8, 9, 10 \quad (7.12)$$

$$c_{cghc3,j} = q-1 \quad \text{for } 11 \leq j \leq 16 \quad (7.13)$$

$$c_{cghc3,j} = 1 \quad \text{for } 17 \leq j \leq 19. \quad (7.14)$$

In [48] we have discussed how cyclic crossing subgraph strips of the square lattice with free transverse boundary conditions reduce, for even and odd length L_x , to cyclic and Möbius strips, respectively. Similarly, here, for even and odd length ℓ , the cyclic crossing subgraph strip of the honeycomb lattice reduces to the cyclic and Möbius strips of this lattice, so that the chromatic polynomial for this cyclic crossing subgraph strip reduces to the respective chromatic polynomial of the cyclic and Möbius strip. With our labelling conventions for the length of the cyclic crossing subgraph strips as compared with the cyclic or Möbius strips of the honeycomb lattice, the cyclic crossing subgraph of even length $\ell = 2m$ (odd length $\ell = 2m + 1$) is identical to the cyclic (Möbius) strip of this lattice of length m , respectively. There is a resultant reduction in the number of $\lambda_{G,j}$'s, from 19 to 14, as a result of the fact that there are five pairs of terms $\lambda_{cghc3,j}$ that differ in sign and have different coefficients, as given above. For the even-length case we thus have the identifications

$$(\lambda_{cghc3,j})^{2m} = (\lambda_{hc3,j})^m \quad (7.15)$$

while for the odd-length case,

$$(\lambda_{cghc3,j})^{2m+1} = \lambda_{cghc3,j}(\lambda_{hc3,j})^m \quad (7.16)$$

so that, for both the even- and odd- ℓ cases for the crossing-subgraph strips, i.e., for both the cyclic and Möbius strips,

$$\lambda_{hc3,1} = (\lambda_{cghc3,j})^2 \quad \text{for } j = 1, 2 \quad (7.17)$$

$$\lambda_{hc3,2} = (\lambda_{cghc3,j})^2 \quad \text{for } j = 3, 4 \quad (7.18)$$

$$\lambda_{hc3,3} = (\lambda_{cghc3,j})^2 \quad \text{for } j = 5, 8 \quad (7.19)$$

$$\lambda_{hc3,4} = (\lambda_{cghc3,j})^2 \quad \text{for } j = 6, 9 \quad (7.20)$$

$$\lambda_{hc3,5} = (\lambda_{cghc3,j})^2 \quad \text{for } j = 7, 10 \quad (7.21)$$

$$\lambda_{hc3,j} = (\lambda_{cghc3,j+5})^2 \quad \text{for } 6 \leq j \leq 14. \quad (7.22)$$

In the case of odd length, we absorb the left-over factor of $\lambda_{cghc3,j}$ in eq. (7.16) in the definition of the coefficients. The relations (7.17)-(7.22) expressing $\lambda_{hc3,j}$'s for the cyclic/Möbius strips as squares of $\lambda_{cghc3,k}$'s are reflected in obvious relations between the algebraic equations for these terms.

In the limit $\ell \rightarrow \infty$, one derives the singular locus \mathcal{B} for the crossing-subgraph strip. As discussed in [48], since one can take this limit on even values of ℓ or, alternatively, on odd values of ℓ , it follows that the singular loci \mathcal{B} for the infinite-length limits of the cyclic and Möbius strips of the honeycomb lattice are the same. Here this already follows from the property that the $\lambda_{G,j}$'s are the same for the cyclic and Möbius strips.

8 Structural Properties of Chromatic Polynomials for Cyclic Strips of the Honeycomb Strip

Let us define $n_P(hc, L_y, d)$ as the number of terms $\lambda_{P, hc, L_y, j}$, each of which has, as its coefficient, the Chebyshev polynomial $c^{(d)}$, in the chromatic polynomial $P(hc, L_y, q)$ of the cyclic strip of the honeycomb lattice of width L_y , denoted hc, L_y . Clearly, the total number, $N_{P, hc, L_y, \lambda}$, of different terms $\lambda_{P, hc, L_y, j}$ in (1.13) for this family of strip graphs is given by

$$N_{P, hc, L_y, \lambda} = \sum_{d=0}^{L_y} n_P(hc, L_y, d) . \quad (8.1)$$

Using the general formulas (6.18) and (6.19) together with the coloring matrix methods that we have discussed in detail in [47], we can calculate the numbers $n_P(hc, L_y, d)$ and $N_{P, hc, L_y, \lambda}$. We find

$$n_P(hc, L_y, d) = 0 \quad \text{for } d > L_y , \quad (8.2)$$

$$n_P(hc, L_y, L_y) = 1 \quad (8.3)$$

and the values $n_P(hc, 2, 0) = 1$, $n_P(hc, 2, 1) = 2$. All other numbers $n_P(hc, L_y, d)$ are then determined by the following recursion relations. For even $L_y \geq 4$

$$n_P(hc, L_y, d) = n_P(hc, L_y - 1, d - 1) + n_P(hc, L_y - 1, d) + n_P(hc, L_y - 1, d + 1) \quad \text{for } d \geq 1 \quad (8.4)$$

while for $d = 0$,

$$n_P(hc, L_y, 0) = n_P(hc, L_y - 1, 1) . \quad (8.5)$$

For odd $L_y \geq 3$

$$n_P(hc, L_y, d) = n_P(hc, L_y - 1, d - 1) + 2n_P(hc, L_y - 1, d) + n_P(hc, L_y - 1, d + 1) \quad \text{for } d \geq 1 \quad (8.6)$$

while for $d = 0$,

$$n_P(hc, L_y, 0) = n_P(hc, L_y - 1, 0) + n_P(hc, L_y - 1, 1) . \quad (8.7)$$

We observe that the recursion relations (8.4) and (8.5) are the same as we found in [47] for the numbers $n_P(L_y, d)$ for cyclic strips of the square and triangular lattices, while eqs. (8.6) and (8.7) are analogous to the recursion relations that we found for the numbers $n_Z(L_y, d)$ for cyclic strips of the square and triangular lattices (in [47] these applied for both even and odd L_y). We also obtain the relations

$$N_{P, hc, L_y, \lambda} = 4N_{P, hc, L_y - 1, \lambda} - 2n_P(hc, L_y - 1, 0) \quad \text{for odd } L_y \geq 3 \quad (8.8)$$

and

$$N_{P, hc, L_y, \lambda} = 3N_{P, hc, L_y - 1, \lambda} - 2n_P(hc, L_y - 1, 0) \quad \text{for even } L_y \geq 4 \quad (8.9)$$

whence

$$N_{P, hc, L_y, \lambda} = 12N_{P, hc, L_y - 2, \lambda} - 8n_P(hc, L_y - 2, 0) - 2n_P(hc, L_y - 2, 1) \quad \text{for } L_y \geq 4 . \quad (8.10)$$

Results for L_y up to 10 are given in Table 2. These may be compared with the analogous calculations that we carried out for cyclic strips of the square and triangular lattices in [47]. For example, the values $N_{P, hc, L_y, \lambda} = 4, 14$ and 36 for $L_y = 2, 3$ and 4 may be contrasted with the numbers $N_{P, G, L_y, \lambda} = 4, 10$ and 26

Table 2: Table of numbers $n_P(hc, L_y, d)$ and their sums, $N_{P, hc, L_y, \lambda}$ for cyclic strips of the honeycomb lattice. Blank entries are zero.

$L_y \downarrow d \rightarrow$	0	1	2	3	4	5	6	7	8	9	10	$N_{P, hc, L_y, \lambda}$
2	1	2	1									4
3	3	6	4	1								14
4	6	13	11	5	1							36
5	19	43	40	22	7	1						132
6	43	102	105	69	30	8	1					358
7	145	352	381	273	137	47	10	1				1346
8	352	878	1006	791	457	194	58	11	1			3748
9	1230	3114	3681	3045	1899	903	321	81	13	1		14288
10	3114	8025	9840	8625	5847	3123	1305	415	95	14	1	40404

for $G = sq, tri$ with the same set of L_y values. It is straightforward to extend these to higher values of L_y , and related results can also be given for Möbius strips of the honeycomb lattice.

From eq. (8.10), it follows that the leading asymptotic behavior of $N_{P, hc, L_y, \lambda}$ (ignoring power-law prefactors) is

$$N_{P, hc, L_y, \lambda} \sim (12)^{L_y/2} = (3.4641\dots)^{L_y} \quad \text{as } L_y \rightarrow \infty. \quad (8.11)$$

This may be contrasted with the leading asymptotic behavior of the corresponding numbers for the cyclic/Möbius strips of the square and triangular lattices [47]

$$N_{P, G, L_y, \lambda} \sim 3^{L_y} \quad \text{for } G = sq, tri \quad \text{as } L_y \rightarrow \infty. \quad (8.12)$$

Regarding the full Potts model partition function, we note that a generalization of the relation (5.1.15) to $C_Z = q^{L_y}$ for the cyclic honeycomb strip with width L_y yields the result $N_{Z, hc, L_y, \lambda} = \binom{2L_y}{L_y}$, similarly to the case with the corresponding strips of the square and triangular lattices.

9 Cylindrical $L_y = 4$ Strip of the Honeycomb Lattice

The first width for which a strip of the honeycomb lattice with cylindrical $= (PBC_y, FBC_x)$ boundary conditions can naturally be defined, satisfying $\Delta_{max} = 3$, is the width $L_y = 4$. A picture of such a lattice is shown in Fig. 20 for length $m = 3$ bricks. In the labelling convention of [35, 37], this would be denoted as $m = 2$; the present convention yields somewhat simpler expressions for the coefficient functions in the numerator of the generating function.

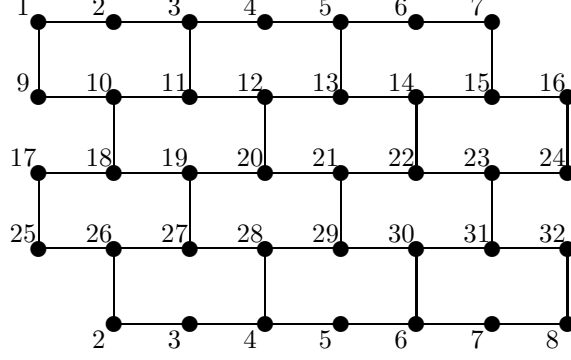


Figure 20: Illustrative strip graph of the honeycomb lattice with width $L_y = 4$, length $m = 3$ bricks and $(PBC_y, FBC_x) =$ cylindrical boundary conditions.

In general, for the strip of the honeycomb lattice with cylindrical (PBC_y, FBC_x) boundary conditions there are $n = 2L_y(m + 1)$ vertices and $e = L_y(3m + 2)$ edges. As before, it is convenient to present the results in terms of a generating function, denoted $\Gamma(G_s, q, x)$, where G_s refers to the type of strip graph. The chromatic polynomial $P((G_s)_m, q)$ is determined as the coefficient in a Taylor series expansion of this generating function in an auxiliary variable z about $z = 0$:

$$\Gamma(G_s, q, z) = \sum_{m=0}^{\infty} P((G_s)_m, q) z^m . \quad (9.1)$$

The generating function $\Gamma(G_s, q, z)$ is a rational function of the form

$$\Gamma(G_s, q, z) = \frac{\mathcal{N}(G_s, q, z)}{\mathcal{D}(G_s, q, z)} \quad (9.2)$$

with

$$\mathcal{N}(G_s, q, z) = \sum_{j=0}^{d_{\mathcal{N}}} A_{G_s, j}(q) z^j \quad (9.3)$$

and

$$\mathcal{D}(G_s, q, z) = 1 + \sum_{j=1}^{d_{\mathcal{D}}} b_{G_s, j}(q) z^j \quad (9.4)$$

where the $A_{G_s, j}$ and $b_{G_s, j}$ are polynomials in q , and $d_{\mathcal{N}} \equiv \deg_z(\mathcal{N})$, $d_{\mathcal{D}} \equiv \deg_z(\mathcal{D})$, In factorized form

$$\mathcal{D}(G_s, q, z) = \prod_{j=1}^{d_{\mathcal{D}}} (1 - \lambda_{G_s, j}(q) z) . \quad (9.5)$$

We find that $\deg_z(\mathcal{N}) = 3$ and $\deg_z(\mathcal{D}) = N_{\lambda} = 4$. The coefficient functions in the numerator and denominator of the generating function are

$$A_0 = q(q-1)(q^6 - 7q^5 + 21q^4 - 35q^3 + 35q^2 - 21q + 7) \quad (9.6)$$

$$\begin{aligned} A_1 &= -q(q-1)(q^{10} - 15q^9 + 103q^8 - 417q^7 + 1074q^6 - 1782q^5 + 1850q^4 \\ &\quad - 1125q^3 + 422q^2 - 246q + 161) \end{aligned} \quad (9.7)$$

$$\begin{aligned}
A_2 = & q(q-1)(4q^{10} - 64q^9 + 460q^8 - 1956q^7 + 5461q^6 - 10497q^5 \\
& + 14128q^4 - 13212q^3 + 8281q^2 - 3203q + 614)
\end{aligned} \tag{9.8}$$

$$A_3 = -4q(q-1)^5(q-2)^2 \tag{9.9}$$

$$b_1 = -q^8 + 12q^7 - 66q^6 + 220q^5 - 496q^4 + 796q^3 - 922q^2 + 734q - 314 \tag{9.10}$$

$$\begin{aligned}
b_2 = & q^{12} - 20q^{11} + 188q^{10} - 1092q^9 + 4344q^8 - 12428q^7 + 26192q^6 \\
& - 41022q^5 + 47597q^4 - 40318q^3 + 24247q^2 - 9782q + 2169
\end{aligned} \tag{9.11}$$

$$\begin{aligned}
b_3 = & -4q^{12} + 80q^{11} - 736q^{10} + 4124q^9 - 15705q^8 + 42922q^7 - 86535q^6 \\
& + 129964q^5 - 144575q^4 + 116374q^3 - 64525q^2 + 22280q - 3680
\end{aligned} \tag{9.12}$$

$$b_4 = 4[(q-1)(q-2)]^4. \tag{9.13}$$

The W function is given as $W = (\lambda_{hc4pf,j})^{1/8}$, where $\lambda_{hc4pf,j}$ is the maximum-magnitude root of the equation

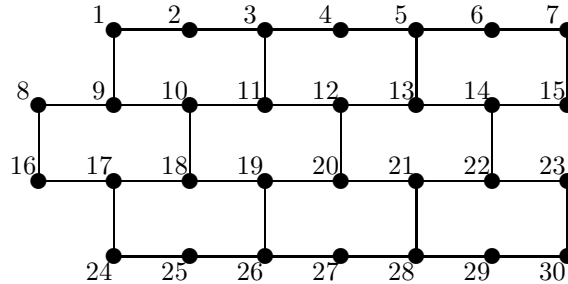
$$\xi^4 + b_1\xi^3 + b_2\xi^2 + b_3\xi + b_4 = 0 \tag{9.14}$$

with the b_j coefficients given in eqs. (9.10)-(9.13).

A plot of the chromatic zeros for a long finite strip of this type is shown in Fig. 21. For this great a length, these zeros give a reasonably accurate indication of the position of the asymptotic locus \mathcal{B} . From our exact analytic results, we find that the locus \mathcal{B} includes arcs and a short interval on the real axis $2.194004 \leq q \leq q_c$, where $q_c = 2.249840$. It is interesting that this value of q_c is just 14 % below the value (5.3.2) for the infinite 2D honeycomb lattice. We also note that the locus \mathcal{B} includes support for $Re(q) < 0$, as is evident from Fig. 21.

10 Free $L_y = 4$ Strip of the Honeycomb Lattice

In general for a strip of the honeycomb lattice with free boundary conditions, width L_y , and m bricks, there are $n = 2(L_y m + L_y - 1)$ vertices and $e = (3L_y - 1)m + 2L_y - 3$ edges. An illustration of the strip of the honeycomb lattice with width $L_y = 4$, length $m = 3$, and free = (FBC_y, FBC_x) boundary conditions is shown in Fig. 22 (in the labelling convention of [35, 37], this would be denoted as length $m = 2$).



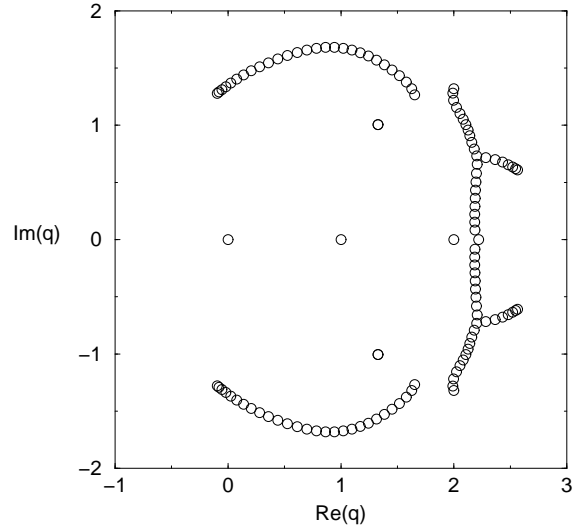


Figure 21: Chromatic zeros for the width $L_y = 4$ strip of the honeycomb lattice with cylindrical boundary conditions, (PBC_y, FBC_x) , for length $m = 14$ (i.e., $n = 120$).

Figure 22: Illustrative strip graph of the honeycomb lattice with width $L_y = 4$, length $m = 3$ bricks and open boundary conditions.

We find that $\deg_x(\mathcal{N}) = 4$ and $\deg_x(\mathcal{D}) = N_\lambda = 5$. The coefficient functions in the numerator and denominator of the generating function are

$$A_0 = q(q-1)^5 \quad (10.1)$$

$$A_1 = -q(q-1)(2q^8 - 22q^7 + 109q^6 - 314q^5 + 566q^4 - 636q^3 + 417q^2 - 133q + 10) \quad (10.2)$$

$$\begin{aligned} A_2 = & q(q-1)^2(q^{11} - 17q^{10} + 133q^9 - 628q^8 + 1975q^7 - 4306q^6 + 6570q^5 \\ & - 6933q^4 + 4921q^3 - 2273q^2 + 683q - 133) \end{aligned} \quad (10.3)$$

$$\begin{aligned} A_3 = & -q(q-1)^2(2q^{11} - 34q^{10} + 268q^9 - 1289q^8 + 4182q^7 - 9547q^6 \\ & + 15548q^5 - 17985q^4 + 14487q^3 - 7811q^2 + 2599q - 424) \end{aligned} \quad (10.4)$$

$$A_4 = 2q(q-1)^5(q-2)(2q^5 - 16q^4 + 49q^3 - 71q^2 + 49q - 12) \quad (10.5)$$

$$b_1 = -(q^2 - 4q + 5)(q^6 - 7q^5 + 22q^4 - 42q^3 + 54q^2 - 47q + 27) \quad (10.6)$$

$$\begin{aligned} b_2 = & 2q^{12} - 36q^{11} + 305q^{10} - 1609q^9 + 5894q^8 - 15827q^7 + 32046q^6 \\ & - 49513q^5 + 58255q^4 - 51198q^3 + 32069q^2 - 12915q + 2555 \end{aligned} \quad (10.7)$$

$$\begin{aligned} b_3 = & -q^{16} + 25q^{15} - 297q^{14} + 2224q^{13} - 11745q^{12} + 46379q^{11} \\ & - 141680q^{10} + 341694q^9 - 658019q^8 + 1016383q^7 - 1256955q^6 \\ & + 1233979q^5 - 945308q^4 + 548423q^3 - 228538q^2 + 61589q - 8161 \end{aligned} \quad (10.8)$$

$$\begin{aligned} b_4 = & (q-1)^2(2q^{14} - 44q^{13} + 456q^{12} - 2951q^{11} + 13318q^{10} - 44313q^9 \\ & + 112043q^8 - 218692q^7 + 331398q^6 - 388712q^5 + 348419q^4 \\ & - 232363q^3 + 109612q^2 - 33033q + 4876) \end{aligned} \quad (10.9)$$

$$b_5 = -2(q-1)^6(q-2)^2(2q^6 - 20q^5 + 83q^4 - 185q^3 + 239q^2 - 175q + 60) . \quad (10.10)$$

The W function is given as $W = (\lambda_{hc4ff,j})^{1/8}$, where $\lambda_{hc4ff,j}$ is the maximum-magnitude root of the equation

$$\xi^5 + b_1\xi^4 + b_2\xi^3 + b_3\xi^2 + b_4\xi + b_5 = 0 \quad (10.11)$$

with the b_j coefficients given in eqs. (10.6)-(10.10).

A plot of the chromatic zeros for a long finite strip of this type is shown in Fig. 23. From our exact analytic results we find that the locus \mathcal{B} includes arcs and a short interval on the real axis $2.078191 \leq q \leq q_c$ where $q_c = 2.099012$.

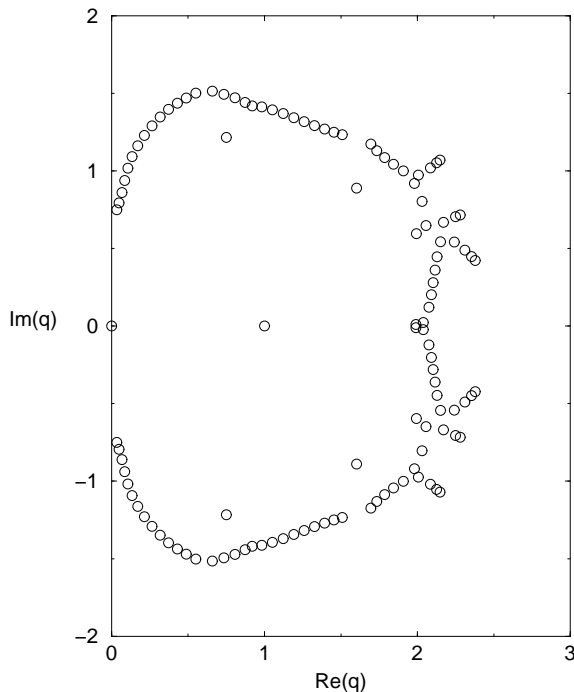


Figure 23: Chromatic zeros for the width $L_y = 4$ strip of the honeycomb lattice with free boundary conditions, (FBC_y, FBC_x) and length $m = 14$ (i.e., $n = 118$).

11 Numerical Values of W

It is of interest to use our new exact results to study further the approach of W to the $L_y \rightarrow \infty$ limit, i.e., the infinite 2D honeycomb lattice. This extends our previous study in [34]. In Table 3 we list values of $W(hc, L_y \times \infty, BC_y, BC_x, q)$ (which, for this range of q , are independent of BC_x), for free and periodic (cylindrical) transverse boundary conditions. These are compared with Monte Carlo measurements of W for the full 2D square lattice, $W(hc, q)$ from [30, 31]. We also list the ratios

$$R_W(\Lambda, L_y, BC_y, q) = \frac{W(\Lambda, L_y, BC_y, q)}{W(\Lambda, q)} \quad (11.1)$$

for the present case, $\Lambda = hc$. In [34] it was proved for a general lattice Λ that the ratio (11.1) approaches unity monotonically for FBC_y . For PBC_y , this approach is nonmonotonic, but more rapid. One sees from Table 3 that for $L_y = 4$ and moderate values of q , say 5 or 6, the agreement of $W(hc, L_y, q)$ for the infinite-length, finite-width open strips with the respective values $W(hc, q)$ for the infinite honeycomb lattice is very good; the ratios are unity to within a few per cent. For the same width $L_y = 4$ and similar q values, the agreement for the cylindrical strip is excellent; the ratios are unity to within a few parts in 10^5 . The agreement, as measured by these ratios, gets better as q increases. This shows that calculations on infinite-length, finite-width strips of the honeycomb lattice with cylindrical boundary conditions provide an excellent approximation to the exact function $W(hc, q)$ for the full 2D honeycomb lattice. This is a very useful result since the latter function has never been calculated exactly. We also give some further values of W or $|W|$ in Table 4.

Table 3: Values of $W(hc, L_y \times \infty, FBC_y, BC_x, q)$, denoted $W(hc, L_y, F, q)$ for short, and $W(hc, L_y \times \infty, PBC_y, BC_x, q)$, denoted $W(hc, L_y, P, q)$ for short, with any BC_x . These are compared with the values for the full 2D honeycomb lattice, $W(hc, q) = W(hc, \infty \times \infty, q)$ for $3 \leq q \leq 10$. For each value of q , the quantities in the upper line are identified at the top and the quantities in the lower line are the values of $R_W(hc, L_y, BC_y, q)$.

q	$W(hc, 2, F, q)$	$W(hc, 3, F, q)$	$W(hc, 4, F, q)$	$W(hc, 4, P, q)$	$W(hc, q)$
3	1.82116 1.097	1.76567 1.064	1.73864 1.047	1.67079 1.0065	1.6600(5) 1
4	2.79468 1.073	2.72942 1.048	2.69737 1.036	2.60443 1.0002	2.6038(7) 1
5	3.78389 1.057	3.71448 1.038	3.68025 1.028	3.57963 1.0000	3.5796(10) 1
6	4.77760 1.046	4.70568 1.031	4.67013 1.023	4.56513 0.9999	4.5654(15) 1
7	5.77336 1.039	5.69973 1.026	5.66327 1.019	5.55529 0.9999	5.5556(17) 1
8	6.77028 1.034	6.69539 1.0225	6.65826 1.017	6.54810 1.0000	6.5479(20) 1
9	7.76793 1.030	7.69208 1.020	7.65443 1.015	7.54259 1.0000	7.5424(22) 1
10	8.76607 1.027	8.68945 1.018	8.65140 1.013	8.53822 1.0000	8.5386(25) 1

Table 4: Values of $W(hc, L_y \times \infty, BC_y, BC_x, q)$ for low integral q and for respective q_c , if such a point exists, where BC_y and BC_x denote the transverse and longitudinal boundary conditions. The notation n in the q_c column means that there is no q_c for this family, i.e., \mathcal{B}_q does not cross the positive real q axis.

L_y	BC_y	BC_x	$ W_{q=0} $	$ W_{q=1} $	$ W_{q=2} $	q_c	$W_{q=q_c}$
2	F	F	1.495	1	1	n	—
3	F	F	1.70	1.26	1	2	1
4	F	F	1.81	1.39	1.09	2.10	1.06
2	F	(T)P	1.495	1.19	1	2	1
3	F	(T)P	1.70	1.35	1	2	1
4	P	F	2.05	1.56	1.19	2.25	1.12

12 Conclusions

In this paper we have presented exact calculations of the partition function of the q -state Potts model and the special case of the $T = 0$ Potts antiferromagnet (chromatic polynomial) on a variety of strips of the honeycomb lattice with fixed width and arbitrarily great length. We have computed the exact free energy and discussed the thermodynamics for the ferromagnetic and antiferromagnetic cases, including the singularities at the zero-temperature critical point of the ferromagnet. These results were compared with those obtained from exact free energy calculations for infinite-length strips of the square and triangular lattices and the differences explained. The W values calculated from the finite-width, infinite-length strips were shown to approach the values for the full 2D honeycomb lattice reasonably rapidly. This was especially dramatic for the $L_y = 4$ strip with periodic transverse (cylindrical) boundary conditions, and the exact results for this strip thus provide a very accurate approximation to the W function for the full 2D honeycomb lattice. This is useful since there is no exact solution for $W(q)$ on the honeycomb lattice for $q > 2$. Generalizing q and temperature to complex values and taking the limit of infinite length, we have studied the locus of singularities \mathcal{B} of the free energy in the q and u planes, and for the $T = 0$ antiferromagnet, the locus \mathcal{B}_q .

Acknowledgment: The research of R. S. was supported in part by the U. S. NSF grant PHY-97-22101.

13 Appendix

13.1 A Remark on Generating Functions

In [35, 36, 37] the methodology on generating function for chromatic polynomials for recursive families of strip graphs was given. For generality, the open strip graphs were taken to be of the symbolic form $G_m = IH^m$, i.e., m -fold repetitions of a subgraph H connected to an initial end graph I . It was proved in [35] that the denominator of the generating function is independent of the end graph I . In [36], a study was carried out of inhomogeneous strip graphs where $I \neq H$. However, if $I = H$, one can simplify the general formalism slightly by redefining the label m via a shift by one unit. Thus, if $I = H$, then the strip denoted symbolically as IH^m is identical to H^{m+1} . The generating function is given in general by equations of the form (9.1)-(9.4). Now in the convention (which is denoted here as C1) of [35, 36, 37], the zeroth-order term, $A_{G_s,0}$ in the expansion (9.1) is the chromatic polynomial for the subgraph I . If $I = H$, as in the homogeneous strips considered here, then it is simpler to use a convention, which we denote C2, according to which the zeroth-order term in the expansion is the chromatic polynomial for one end (say the left-hand end) of the strip. For example, for the width L_y strip of the square lattice, in conventions C1 and C2, $A_{sq,L_y,0}$ would be the chromatic polynomial for a column of squares of height L_y and the line graph T_{L_y} , respectively, i.e., $A_{sq,L_y,0} = q(q-1)(q^2 - 3q + 3)^{L_y-1}$ and $A_{sq,L_y,0} = q(q-1)^{L_y-1}$. To distinguish these two conventions, let us, in this subsection, append a prime to the numerator defined with the latter convention C2, i.e.,

$$\mathcal{N}(G_s, q, z)' = \sum_{j=0}^{d_{\mathcal{N}}} A'_{G_s,j}(q)z^j . \quad (13.1.1)$$

Thus, for $m \geq 1$, the m 'th term in the expansion of the generating function $\Gamma(G_s, q, z)'$ is the same as the $(m-1)$ 'th term in the expansion of the generating function $\Gamma(G_s, q, z)$. While the denominators are the

same, the coefficient functions in the numerators are related according to

$$A'_{G_s,j} = A_{G_s,j-1} + A'_{G_s,0} b_{G_s,j} \quad \text{for } j \geq 1. \quad (13.1.2)$$

Similar relations hold for the generating functions of the full Potts model partition function and equivalently the Tutte polynomial.

We give some simple illustrations next. For the $L_y = 2$ strip of the square lattice with free boundary conditions and C1,

$$\Gamma_{P,sq,2} = \frac{q(q-1)D_4}{1-D_4z} \quad (13.1.3)$$

while with convention C2

$$\Gamma'_{P,sq,2} = \frac{q(q-1)}{1-D_4z}. \quad (13.1.4)$$

For the $L_y = 3$ strip of the square lattice with free boundary conditions and labelling convention C1 [35]

$$A_{P,sq3,0} = q(q-1)D_4^2 \quad (13.1.5)$$

$$A_{P,sq3,1} = -q(q-1)^3(q^3 - 6q^2 + 13q - 11) \quad (13.1.6)$$

while for convention C2,

$$A'_{P,sq3,0} = q(q-1)^2 \quad (13.1.7)$$

$$A'_{P,sq3,1} = -q(q-1)(q^2 - 3q + 1) \quad (13.1.8)$$

and in both cases

$$b_{P,sq3,1} = -(q-2)(q^2 - 3q + 5) \quad (13.1.9)$$

$$b_{P,sq3,2} = (q-1)(q^3 - 6q^2 + 13q - 11). \quad (13.1.10)$$

Similarly, with convention C1, the generating functions for the Tutte polynomials for the $L_y = 2$ open strip of the square and triangular lattices are

$$\Gamma_{T,sq,2} = \frac{(y+x+x^2+x^3) - yx^3z}{1 - (y+1+x+x^2)z + yx^2z^2} \quad (13.1.11)$$

and

$$\Gamma_{T,tri,2} = \frac{x(x+1)^2 + 2xy + y(y+1) - x^3y^2z}{1 - [(x+1)^2 + y(y+2)]z + x^2y^2z^2} \quad (13.1.12)$$

while with convention C2, they have the simpler forms

$$\Gamma'_{T,sq,2} = \frac{x+y(1-x)z}{1 - (y+1+x+x^2)z + yx^2z^2} \quad (13.1.13)$$

and

$$\Gamma'_{T,tri,2} = \frac{x-y(yx-y-1)z}{1 - [(x+1)^2 + y(y+2)]z + x^2y^2z^2} \quad (13.1.14)$$

and so forth for other lattice strips. We shall use convention C2 here.

13.2 Connection Between Potts Model Partition Function and Tutte Polynomial

The formulas relating the Potts model partition function $Z(G, q, v)$ and the Tutte polynomial $T(G, x, y)$ were given in [14] and hence we shall be brief here. The Tutte polynomial of G , $T(G, x, y)$, is given by [7]-[9]

$$T(G, x, y) = \sum_{G' \subseteq G} (x-1)^{k(G')-k(G)} (y-1)^{c(G')} \quad (13.2.1)$$

where $k(G')$, $e(G')$, and $n(G') = n(G)$ denote the number of components, edges, and vertices of G' , and

$$c(G') = e(G') + k(G') - n(G') \quad (13.2.2)$$

is the number of independent circuits in G' . For the graphs of interest here, $k(G) = 1$. Now let

$$x = 1 + \frac{q}{v} \quad (13.2.3)$$

and

$$y = a = v + 1 \quad (13.2.4)$$

so that

$$q = (x-1)(y-1) . \quad (13.2.5)$$

Then

$$Z(G, q, v) = (x-1)^{k(G)} (y-1)^{n(G)} T(G, x, y) . \quad (13.2.6)$$

For a planar graph G the Tutte polynomial satisfies the duality relation

$$T(G, x, y) = T(G^*, y, x) \quad (13.2.7)$$

where G^* is the (planar) dual to G . As discussed in [14], the Tutte polynomial for recursively defined graphs comprised of m repetitions of some subgraph has the form

$$T(G_m, x, y) = \sum_{j=1}^{N_\lambda} c_{T,G,j} (\lambda_{T,G,j})^m . \quad (13.2.8)$$

13.3 Open $L_y = 2$ Strip of the Honeycomb Lattice

The generating function for the Tutte polynomial for the open strip of the honeycomb lattice comprised of m bricks, denoted S_m , is

$$\Gamma_T(S_m, x, y, z) = \sum_{m=0}^{\infty} T(S_m, x, y) z^m . \quad (13.3.1)$$

We calculate

$$\Gamma_T(S, x, y, z) = \frac{x + y(1-x)z}{1 - (x^4 + x^3 + x^2 + x + y + 1)z + yx^4z^2} . \quad (13.3.2)$$

This yields

$$\lambda_{T,S,(1,2)} = \frac{1}{2} \left[x^4 + x^3 + x^2 + x + y + 1 \pm \sqrt{R_{TS}} \right] \quad (13.3.3)$$

where

$$\begin{aligned} R_{TS} = & x^8 + 2x^7 + 3x^6 - 2yx^4 + 4x^5 + 2yx^3 + 5x^4 + 2yx^2 \\ & + 4x^3 + y^2 + 2yx + 3x^2 + 2y + 2x + 1 . \end{aligned} \quad (13.3.4)$$

13.4 Cyclic and Möbius $L_y = 2$ Strips of the Honeycomb Lattice

We calculate

$$T(L_m, x, y) = \sum_{j=1}^6 c_{T,L,j} (\lambda_{T,L,j})^m \quad (13.4.1)$$

and

$$T(ML_m, x, y) = \sum_{j=1}^6 c_{T,ML,j} (\lambda_{T,ML,j})^m \quad (13.4.2)$$

where

$$\lambda_{T,ML,j} = \lambda_{T,L,j}, \quad j = 1, \dots, 6 \quad (13.4.3)$$

$$\lambda_{T,L,1} = 1 \quad (13.4.4)$$

$$\lambda_{T,L,2} = x^2 \quad (13.4.5)$$

$$\lambda_{T,L,(3,4)} = \frac{1}{2} \left[x^2 + 2x + y + 2 \pm \sqrt{R_{T34}} \right] \quad (13.4.6)$$

with

$$R_{T34} = x^4 + 4x^3 - 2x^2y + 8x^2 + 4xy + 8x + y^2 + 4y + 4 \quad (13.4.7)$$

$$\lambda_{T,L,5} = \lambda_{T,S,1}, \quad \lambda_{T,L,6} = \lambda_{T,S,2} \quad (13.4.8)$$

where $\lambda_{T,S,1}$ and $\lambda_{T,S,2}$ were given above.

It is convenient to extract a common factor from the coefficients:

$$c_{T,G,j} \equiv \frac{\bar{c}_{T,G,j}}{x-1}, \quad G = L, ML. \quad (13.4.9)$$

Of course, although the individual terms contributing to the Tutte polynomial are thus rational functions of x rather than polynomials in x , the full Tutte polynomial is a polynomial in both x and y . We have

$$\bar{c}_{T,L,j} = c_{Z,L,j} \quad \text{for } 1 \leq j \leq 6. \quad (13.4.10)$$

Thus, in terms of the variables x and y , e.g., $\bar{c}_{T,L,j} = q - 1 = xy - x - y$ for $j = 2, 3, 4$, etc. Further,

$$\bar{c}_{T,ML,j} = c_{Z,ML,j} \quad \text{for } 1 \leq j \leq 6. \quad (13.4.11)$$

13.5 Special Values of Tutte Polynomials for Strips of the Honeycomb Lattice

For a given graph $G = (V, E)$, at certain special values of the arguments x and y , the Tutte polynomial $T(G, x, y)$ yields quantities of basic graph-theoretic interest [9]-[12]. We recall some definitions: a spanning subgraph was defined at the beginning of the paper; a tree is a connected graph with no cycles; a forest is a graph containing one or more trees; and a spanning tree is a spanning subgraph that is a tree. We recall that the graphs G that we consider are connected. Then the number of spanning trees of G , $N_{ST}(G)$, is

$$N_{ST}(G) = T(G, 1, 1), \quad (13.5.1)$$

the number of spanning forests of G , $N_{SF}(G)$, is

$$N_{SF}(G) = T(G, 2, 1), \quad (13.5.2)$$

the number of connected spanning subgraphs of G , $N_{CSSG}(G)$, is

$$N_{CSSG}(G) = T(G, 1, 2) , \quad (13.5.3)$$

and the number of spanning subgraphs of G , $N_{SSG}(G)$, is

$$N_{SSG}(G) = T(G, 2, 2) . \quad (13.5.4)$$

An elementary theorem (e.g., [17]) is that

$$N_{SSG}(G) = 2^{e(G)} . \quad (13.5.5)$$

From our calculations of Tutte polynomials, we find that for the $L_y = 2$ strip of the honeycomb lattice with free boundary conditions, S_m ,

$$N_{ST}(S_m) = \frac{1}{4\sqrt{2}} \left[(3 + 2\sqrt{2})^{m+1} - (3 - 2\sqrt{2})^{m+1} \right] \quad (13.5.6)$$

$$N_{SF}(S_m) = \frac{1}{8\sqrt{15}} \left[(31 + 8\sqrt{15})[4(4 + \sqrt{15})]^m - (31 - 8\sqrt{15})[4(4 - \sqrt{15})]^m \right] \quad (13.5.7)$$

$$N_{CSSG}(S_m) = \frac{1}{\sqrt{41}} \left[\left(\frac{7 + \sqrt{41}}{2} \right)^{m+1} - \left(\frac{7 - \sqrt{41}}{2} \right)^{m+1} \right] \quad (13.5.8)$$

$$N_{SSG}(S_m) = 2^{e(S_m)} = 2^{5m+1} . \quad (13.5.9)$$

For the $L_y = 2$ cyclic and Möbius strips of the honeycomb lattice, L_m and ML_m , we find, with $\eta_G = \pm 1$ for L_m and ML_m , respectively:

$$N_{ST}(G_m) = m \left[-2\eta_G + (3 + 2\sqrt{2})^m + (3 - 2\sqrt{2})^m \right] \quad \text{for } G_m = L_m, ML_m \quad (13.5.10)$$

$$\begin{aligned} N_{SF}(G_m) &= \eta_G(1 - 2^{2m}) - \left[\left(\frac{11 + \sqrt{105}}{2} \right)^m + \left(\frac{11 - \sqrt{105}}{2} \right)^m \right] \\ &\quad + \left\{ [4(4 + \sqrt{15})]^m + [4(4 - \sqrt{15})]^m \right\} \text{for } G_m = L_m, ML_m \end{aligned} \quad (13.5.11)$$

$$\begin{aligned} N_{CSSG}(L_m) &= N_{CSSG}(ML_m) - 4m - 1 \\ &= -2(m + 1) + \left[1 + m \left(1 - \frac{1}{\sqrt{41}} \right) \right] \left(\frac{7 + \sqrt{41}}{2} \right)^m \\ &\quad + \left[1 + m \left(1 + \frac{1}{\sqrt{41}} \right) \right] \left(\frac{7 - \sqrt{41}}{2} \right)^m \end{aligned} \quad (13.5.12)$$

$$N_{SSG}(L_m) = N_{SSG}(ML_m) = 2^{e(L_m)} = 2^{5m} . \quad (13.5.13)$$

Since $T(G_m, x, y)$ grows exponentially as $m \rightarrow \infty$ for the families $G_m = S_m$ and L_m for $(x, y) = (1, 1)$, $(2, 1)$, $(1, 2)$, and $(2, 2)$, it is natural to define the corresponding constants

$$z_{set}(\{G\}) = \lim_{n(G) \rightarrow \infty} n(G)^{-1} \ln N_{set}(G), \quad set = ST, SF, CSSG, SSG \quad (13.5.14)$$

where, as above, the symbol $\{G\}$ denotes the limit of the graph family G as $n(G) \rightarrow \infty$ (and the z here should not be confused with the auxiliary expansion variable in the generating function (13.3.1) or the Potts partition function $Z(G, q, v)$.) General inequalities for these were given in [14]. Our results yield

$$z_{ST}(\{G\}) = \frac{1}{4} \ln(3 + 2\sqrt{2}) \simeq 0.440687 \quad \text{for } G = S, L, ML \quad (13.5.15)$$

$$z_{SF}(\{G\}) = \frac{1}{4} \ln[4(4 + \sqrt{15})] \simeq 0.862433 \quad \text{for } G = S, L, ML \quad (13.5.16)$$

$$z_{CSSG}(\{G\}) = \frac{1}{4} \ln\left(\frac{7 + \sqrt{41}}{2}\right) \simeq 0.475585 \quad \text{for } G = S, L, ML \quad (13.5.17)$$

and

$$z_{SSG}(\{G\}) = (5/4) \ln 2 \simeq 0.866434 \quad \text{for } G = S, L, ML \quad (13.5.18)$$

Another comparison of interest is the ratio of z_{ST} for these $L_y = 2$ strips with z_{ST} for the full 2D honeycomb lattice, which has the value [66]

$$z_{ST}(hc) = \frac{1}{2} z_{ST}(tri) = \frac{3\sqrt{3}}{2\pi} (1 - 5^{-2} + 7^{-2} - 11^{-2} + 13^{-2} - \dots) = 0.807664868\dots \quad (13.5.19)$$

namely,

$$\frac{z_{ST}(\{L\})}{z_{ST}(hc)} \simeq 0.545631. \quad (13.5.20)$$

In the case of z_{ST} , it is also of interest to compare the results with a general upper bound [10]

$$z_{ST}(\{G\}) \leq z_{ST,upper}(\{G\}) = \ln \Delta_{eff}(\{G\}) \quad (13.5.21)$$

where the effective coordination number (degree) was defined above in eq. (4.4). For this comparison we define the ratio

$$r_{ST}(\{G\}) = \frac{z_{ST}(\{G\})}{z_{ST,upper}(\{G\})}. \quad (13.5.22)$$

We find

$$r_{ST}(\{G\}) = \frac{\ln(3 + 2\sqrt{2})}{4 \ln(\frac{5}{2})}. \quad \text{for } G = S, L, ML \quad (13.5.23)$$

We compare these results with others that we have obtained for infinite-length strips of other lattices [14, 16] in Table 5. We recall that the strip of the triangular lattice is constructed by starting with a strip of the square lattice and adding edges joining the lower left to upper right vertex of each square. For uniformity, when comparing the values of $z_{ST}(\{G\})$ to upper bounds, we use the general bound (13.5.21). It should be remarked, however, that in contrast to the strip graphs of the honeycomb lattice considered here, the cyclic $L_y = 2$ strip graphs of the square and triangular lattice and the infinite-length open strips of these lattices are Δ -regular, and hence one can apply a somewhat more restrictive upper bound, as discussed in [67].

The (planar) dual of L_m can be described as follows. In mathematical graph theory, the ‘‘join’’ $G + H$ of the graphs G and H is defined as the graph with the vertex set $V = V_G + V_H$ and edge set E comprised

Table 5: $z_s(\{G\})$ for the $L_x \rightarrow \infty$ limit of the width $L_y = 2$ strips of the (i) honeycomb lattice, (ii) square lattice, and (iii) triangular lattice.

$z_s(\{G\})$	$\{G\} = hc$	$\{G\} = sq$	$\{G\} = tri$
$z_{ST}(\{G\})$	$(1/4) \ln(3 + 2\sqrt{2})$ = 0.440687	$(1/2) \ln(2 + \sqrt{3})$ = 0.658479	$(1/2) \ln[(7 + 3\sqrt{5})/2]$ = 0.962424
$r_{ST}(\{G\})$	0.4809	0.5994	0.6942
$z_{SF}(\{G\})$	$(1/4) \ln[4(4 + \sqrt{15})]$ = 0.862433	$(1/2) \ln[2(2 + \sqrt{3})]$ = 1.005053	$(1/2) \ln[2(3 + 2\sqrt{2})]$ = 1.227947
$z_{CSSG}(\{G\})$	$(1/4) \ln[(7 + \sqrt{41})/2]$ = 0.475585	$(1/2) \ln[(5 + \sqrt{17})/2]$ = 0.758832	$(1/2) \ln[2(3 + 2\sqrt{2})]$ = 1.227947
$z_{SSG}(\{G\})$	$(5/4) \ln 2$ = 0.866434	$(3/2) \ln 2$ = 1.039721	$2 \ln 2$ = 1.386294

of the edges of G and H together with edges joining each vertex of G to each vertex of H . Further, the complete graph K_p is defined as the graph with p vertices such that each vertex is connected by an edge to every other vertex. The complement \bar{K}_p of K_p is the graph composed of p disjoint vertices and no edges. Now consider the join $\bar{K}_2 + C_m$, where C_m is the circuit graph with m vertices. Change each of the edges connecting the two vertices of the \bar{K}_2 to the vertices of the circuit graph C_m to double edges. This yields a multigraph that we shall denote as $\bar{K}_2(+)_e2C_m$, where the symbol $G(+)_e\ell H$ means that one replaces each edge joining a vertex of G with a vertex of H by ℓ such edges. Then the (planar) dual of L_m^* is

$$L_m^* = \bar{K}_2(+)_e2C_m . \quad (13.5.24)$$

The planar dual of S_m is the graph composed of the join of a single vertex \bar{K}_1 with the line graph T_m modified so that each edge connecting the external vertex to the $(m - 2)$ internal vertices of the line graph is replaced by a 4-fold multiple edge, and the edges connecting this external vertex to the two end vertices of the line graph are replaced by 5-fold multiple edges. Thus, our calculations of various graph-theoretic quantities for L_m and S_m also determine those for L_m^* and S_m^* by eq. (13.2.7). Note that this relation does not apply for the Möbius strips since they are not planar.

References

- [1] R. B. Potts, Proc. Camb. Phil. Soc. **48** (1952) 106.
- [2] F. Y. Wu, Rev. Mod. Phys. **54** (1982) 235.
- [3] G. D. Birkhoff, Ann. of Math. **14** (1912) 42.
- [4] H. Whitney, Ann. of Math. **33** (1932) 688.
- [5] P. W. Kasteleyn and C. M. Fortuin, J. Phys. Soc. Jpn. **26** (1969) (Suppl.) 11.
- [6] C. M. Fortuin and P. W. Kasteleyn, Physica **57** (1972) 536.
- [7] W. T. Tutte, Can. J. Math. **6** (1954) 80.
- [8] W. T. Tutte, J. Combin. Theory **2** (1967) 301.

- [9] W. T. Tutte, “Chromials”, in Lecture Notes in Math. v. 411 (1974) 243; *Graph Theory*, vol. 21 of Encyclopedia of Mathematics and Applications (Addison-Wesley, Menlo Park, 1984).
- [10] N. L. Biggs, *Algebraic Graph Theory* (2nd ed., Cambridge Univ. Press, Cambridge, 1993).
- [11] D. J. A. Welsh, *Complexity: Knots, Colourings, and Counting*, London Math. Soc. Lect. Note Ser. 186 (Cambridge University Press, Cambridge, 1993).
- [12] B. Bollobás, *Modern Graph Theory* (Springer, New York, 1998).
- [13] R. Shrock, in the *Proceedings of the 1999 British Combinatorial Conference, BCC99*, Discrete Math., in press (cond-mat/9908387).
- [14] R. Shrock, Physica A **283** (2000) 388.
- [15] H. Kluepfel and R. Shrock, YITP-99-32; H. Kluepfel, Stony Brook thesis (July, 1999).
- [16] S.-C. Chang and R. Shrock, Physica A, in press (cond-mat/0004181).
- [17] S.-C. Chang and R. Shrock, cond-mat/0007505.
- [18] M. Aizenman and E. H. Lieb, J. Stat. Phys. **24** (1981) 279.
- [19] Y. Chow and F. Y. Wu, Phys. Rev. **B36** (1987) 285.
- [20] R. C. Read, J. Combin. Theory **4** (1968) 52.
- [21] R. C. Read and W. T. Tutte, “Chromatic Polynomials”, in *Selected Topics in Graph Theory, 3*, eds. L. W. Beineke and R. J. Wilson (Academic Press, New York, 1988.).
- [22] R. Shrock and S.-H. Tsai, Phys. Rev. **E55** (1997) 5165.
- [23] N. L. Biggs, R. M. Damerell, and D. A. Sands, J. Combin. Theory B **12** (1972) 123.
- [24] N. L. Biggs and G. H. Meredith, J. Combin. Theory B **20** (1976) 5.
- [25] N. L. Biggs, Bull. London Math. Soc. **9** (1976) 54.
- [26] S. Beraha, J. Kahane, and N. Weiss, J. Combin. Theory B **27** (1979) 1.
- [27] S. Beraha, J. Kahane, and N. Weiss, J. Combin. Theory B **28** (1980) 52.
- [28] R. C. Read, in Proc. 3rd Caribbean Conf. on Combin. and Computing (1981).
- [29] R. C. Read, Proc. 5th Caribbean Conf. on Combin. and Computing (1988).
- [30] R. Shrock and S.-H. Tsai, Phys. Rev. **E55** (1997) 6791.
- [31] R. Shrock and S.-H. Tsai, Phys. Rev. **E56** (1997) 1342, 2733, 4111.
- [32] R. Shrock and S.-H. Tsai, Phys. Rev. **E56** (1997) 3935.
- [33] J. Salas and A. Sokal, J. Stat. Phys. **86** (1997) 551.
- [34] R. Shrock and S.-H. Tsai, Phys. Rev. **E58** (1998) 4332; cond-mat/9808057.

- [35] M. Roček, R. Shrock, and S.-H. Tsai, *Physica* **A252** (1998) 505.
- [36] M. Roček, R. Shrock, and S.-H. Tsai, *Physica* **A259** (1998) 367.
- [37] R. Shrock and S.-H. Tsai, *Physica* **A259** (1998) 315.
- [38] R. Shrock and S.-H. Tsai, *J. Phys. A Lett.* **32** (1999) L195.
- [39] R. Shrock and S.-H. Tsai, *Phys. Rev.* **E60** (1999) 3512.
- [40] R. Shrock and S.-H. Tsai, *Physica A* **275** (1999) 429.
- [41] R. Shrock and S.-H. Tsai, *J. Phys. A* **32** (1999) 5053.
- [42] N. L. Biggs, LSE report LSE-CDAM-99-03 (May 1999), to appear.
- [43] R. Shrock, *Phys. Lett.* **A261** (1999) 57.
- [44] N. L. Biggs and R. Shrock, *J. Phys. A (Letts.)* **32** (1999) L489.
- [45] S.-C. Chang and R. Shrock, Stony Brook preprints YITP-SB-99-50,58.
- [46] S.-C. Chang and R. Shrock, *Physica A*, in press (cond-mat/0004161).
- [47] S.-C. Chang and R. Shrock, *Physica A*, in press (cond-mat/0005232).
- [48] S.-C. Chang and R. Shrock, cond-mat/0007491.
- [49] V. Matveev and R. Shrock, *J. Phys. A* **28** (1995) 1557.
- [50] V. Matveev and R. Shrock, *J. Phys. A* **29** (1996) 803.
- [51] V. Matveev and R. Shrock, *Phys. Lett.* **A204** (1995) 353.
- [52] D. Kim and R. Joseph, *J. Phys. C* **7** (1974) L167.
- [53] T. W. Burkhardt and B. W. Southern, *J. Phys. A* **11** (1978) L247.
- [54] R. Shrock and S.-H. Tsai, *J. Phys. A* **30** (1997) 495.
- [55] J. Salas, *J. Phys. A* **31** (1998) 5969.
- [56] H. Feldmann, R. Shrock, and S.-H. Tsai, *J. Phys. A* **30** (1997) L663.
- [57] H. Feldmann, R. Shrock, and S.-H. Tsai, *Phys. Rev.* **E57** (1998) 1335.
- [58] M. E. Fisher, *Lectures in Theoretical Physics* (Univ. of Colorado Press, 1965), vol. 7C, p. 1.
- [59] R. Abe, *Prog. Theor. Phys.* **38** (1967) 322.
- [60] C. N. Yang and T. D. Lee, *Phys. Rev.* **87** (1952) 404.
- [61] T. D. Lee and C. N. Yang, *ibid.* **87** (1952) 410.
- [62] H. Feldmann, A. J. Guttmann, I. Jensen, R. Shrock, and S.-H. Tsai, *J. Phys. A* **31** (1998) 2287.

- [63] C. N. Chen, C. K. Hu, and F. Y. Wu, Phys. Rev. Lett. **76** (1996) 169.
- [64] F. Y. Wu, G. Rollet, H. Y. Huang, J.-M. Maillard, C. K. Hu, and C. N. Chen, Phys. Rev. Lett. **76** (1996) 173.
- [65] V. Matveev and R. Shrock, Phys. Rev. Phys. Rev. **E54** (1996) 6174.
- [66] F. Y. Wu, J. Phys. A **10** (1977) L113.
- [67] R. Shrock and F. Y. Wu, J. Phys. A **33** (2000) 3881.